SCIENCE CHINA
Chemistry

•REVIEWS•

May 2023 Vol.66 No.5: 1318–1335
https://doi.org/10.1007/s11426-022-1529-y

Molecular insights of nanozymes from design to catalytic mechanism

Yuan Xu, Zhixin Zhou, Nankai Deng, Kangchun Fu, Caixia Zhu, Qing Hong, Yanfei Shen, Songqin Liu & Yuanjian Zhang*

Jiangsu Engineering Laboratory of Smart Carbon-Rich Materials and Device, Jiangsu Province Hi-Tech Key Laboratory for Bio-Medical Research, School of Chemistry and Chemical Engineering, Medical School, Southeast University, Nanjing 211189, China

Received December 7, 2022; accepted February 1, 2023; published online February 9, 2023

Emerging as cost-effective potential alternatives to natural enzymes, nanozymes have attracted increasing interest in broad fields. To exploit the in-depth potential of nanozymes, rational structural engineering and explicit catalytic mechanisms at the molecular scale are required. Recently, impressive progress has been made in mimicking the characteristics of natural enzymes by constructing metal active sites, binding pockets, scaffolds, and delicate allosteric regulation. Ingenious in-depth studies have been conducted with advances in structural characterization and theoretical calculations, unveiling the "black box" of nanozyme-catalytic mechanisms. This review introduces the state-of-art synthesis strategies by learning from the natural enzyme counterparts and summarizes the general overview of the nanozyme mechanism with a particular emphasis on the adsorbed intermediates and descriptors that predict the nanozyme activity. The emerging activity assessment methodology that illustrates the relationship between electrochemical oxygen reduction and enzymatic oxygen reduction is discussed with up-to-date advances. Future opportunities and challenges are presented in the end to spark more profound work and attract more researchers from various backgrounds to the flourishing field of nanozymes.

nanozyme, mechanism, descriptor, free-ROS, bound-ROS

Citation: Xu Y, Zhou Z, Deng N, Fu K, Zhu C, Hong Q, Shen Y, Liu S, Zhang Y. Molecular insights of nanozymes from design to catalytic mechanism. *Sci China Chem*, 2023, 66: 1318–1335, https://doi.org/10.1007/s11426-022-1529-y

1 Introduction

Millions of years of natural evolution have endowed enzymes with incredible efficiency, high selectivity, and specificity derived from refined hierarchical structures at the nanoscale. However, great challenges remain in derivative applications owing to the fragile nature of the structure and the difficulty in preparation and separation, thus making natural enzymes susceptible to harsh conditions and expensive.

Since the pioneering report of Fe_3O_4 nanoparticles with peroxidase (POD)-like activity in 2007 [1], nanomaterials with intriguing enzyme-like functions have triggered extensive interest in bridging nanotechnology and biocatalysis. Since then, a rich toolbox of nanomaterials, such as metallic [2,3], metal oxides [4–7], carbon-based materials [8], and metal-organic frameworks (MOFs) [9] has been developed with enzyme-like activities and is now collectively termed nanozymes [10].

Owing to their structural diversity, unique physiochemical properties, and high stability, nanozymes have shown broad applicability (Scheme 1). For instance, nanozymes with oxidase (OXD)-like and POD-like activities can catalyze various substrates under physiological conditions, facilitating their applications in multiplatform-based biosensing and bioimaging [11]. They are also capable of catalyzing the

*Corresponding author (email: Yuanjian.Zhang@seu.edu.cn)

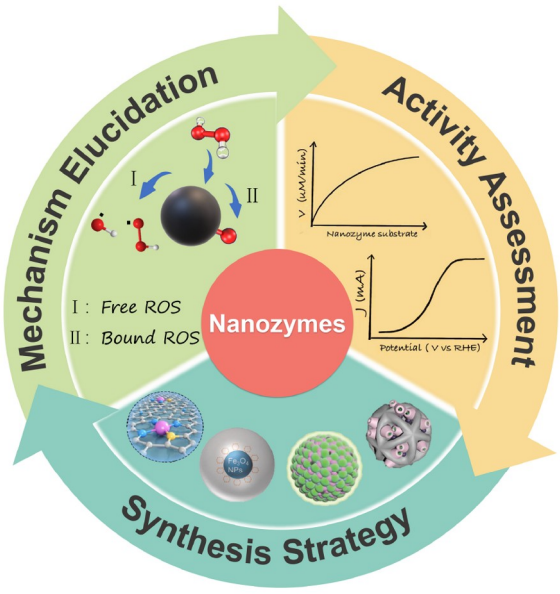

Scheme 1 An overview of synthesis strategy, mechanism elucidation and activity assessment for nanozymes (color online).

formation of cytotoxic reactive oxygen species (ROS), benefitting to antibacterial treatment [12,13], tumor therapy [14,15], and the emerging SARS-coronavirus 2 elimination [16]. Catalase (CAT)-like and superoxide dismutase (SOD)-like nanozymes are effective for treating oxidative stress-related diseases [17], such as inflammatory disease [18], Alzheimer's disease [19] and Parkinson's disease [20]. In particular, after rational molecular structural engineering by simulating enzyme counterparts, nanozymes have been expanded to include haloperoxidase [21,22], hydrolase [23–25], lyase [26], and isomerase [27]. New possibilities have been sparked in pollutant treatment [28,29], drug delivery [30], and metabolism [31], enhancing crop stress resilience [32], even for industrial applications that were previously unavailable in biology [33,34].

Despite great success in the discovery and application of new nanozymes, several challenges still need to be addressed to fully realize their potential [35]. For instance, perusing nanozymes with high catalytic performance and selectivity is a long topic. Moreover, elucidating the catalytic mechanism has been a long-standing problem, and the unambiguous delineation of the molecular structure–catalytic activity relationship remains a formidable challenge. Nanozymes thus present a fertile field for further academic studies, and many groups including our group have investigated them at a molecular scale. A basic understanding of their inherent molecular structural characteristics is necessary for their future development toward real-world applicability. Many breakthroughs have been achieved in nanozyme molecular structure engineering, including biomimetic strategies to imitate the architecture and function of natural enzymes, such as introducing metal active sites, providing close proximity binding pockets, fabricating efficient substrate channeling of nanozymes using biomimetic scaffolds, and simulating regulation patterns. Furthermore, with the development of fine structure characterization and theoretical calculations, ingenious in-depth research has been conducted regarding the real active sites, underlying mechanisms [4], detailed reaction steps, and adsorbed intermediates of nanozymes. Through the collaboration of theoretical simulations and experiments, the "black box" of nanozyme origin has gradually been unveiled.

The rapid development aiming at the above subjects has brought thousands of articles in the last five years along with many outstanding review articles regarding the rational synthesis strategies by surface engineering [36,37], new types [38–40], diverse applications [11,41], and catalytic mechanisms of specific nanozymes [42–46]. To be notified, a comprehensive review first summarized the bio-inspired strategies of nanozymes by introducing enzyme-like cofactors and active centers [47]. These papers provide informative summaries and comments that shed light on many aspects of the current and potential future development of nanozymes. By contrast, as a supplement to previous summaries, this review presents a different perspective focusing on the molecule level. It introduces the state-of-art synthesis strategies by learning from the natural enzyme counterparts and summarizes the general overview of the nanozyme mechanism with a particular emphasis on the adsorbed intermediates and descriptors that predict nanozyme activity. The emerging activity assessment methodology that illustrates the relationship between electrochemical oxygen reduction and enzymatic oxygen reduction is discussed with up-to-date advances. Current challenges and future opportunities for nanozymes are provided. We hope this review will spark more profound work and attract more researchers from various backgrounds to tap the in-depth potential of nanozymes.

2 Biomimetic structural design in molecular-scale

The long evolution process endows enzymes with tailored and fine microstructures. Even though the mode of functions is far from completely known, the booming development of enzymology and crystallography endows us with a profound understanding of the geometric characteristics and action patterns of enzymes: the intrinsic activity, selectivity, and substrate scope of enzymes are achieved by a sophisticated interplay among active-site loops, substrate-binding pockets, folding scaffolds, allosteric regulators, *etc*., which could be translated into general principles in fabricating nanozyme. Substantial research efforts are directed to mimic these features of native enzymes using bio-inspired strategies, which

were defined as a long-term "holy grail" in chemistry. Indeed, ingenious studies have been reported as nanozymes to realize the highly efficient catalytic activity, selectivity, and synergistic working mechanisms of natural enzymes. For instance, the activity of nanozymes could be remarkably improved by integrating enzyme-like metal active sites into the nanozymes. For example, by adding a hemin-like Fe–N_4 active site to graphene, a 700-fold enhancement over the parent graphene was achieved [48]. By further combining Fe–N_4 active sites as the prosthetic group and Fe clusters as cofactors, multiple enzyme-like activities are comparable to natural peroxisome [49]. Expanded Rh–N_4 showed a 20-fold improved affinity compared to natural catalase by imitating the atomic coordination structures of active sites [50]. The specificity of nanozymes can be achieved by introducing enzyme-like binding pockets. For example, coating Fe_3O_4 nanozymes with molecule-imprinted polymers led to a nearly 100-fold increase in substrate specificity [51], and the incorporation of sequence-specific aptamer binding strands into carbon dot nanozymes enables selective substrate binding and concentration [52]. The efficient substrate channeling of nanozymes can be fulfilled by learning from the enzyme scaffold [53]. Furthermore, the activity of nanozymes can be controlled by simulating the regulatory functions of enzymes [54]. Accordingly, as illustrated in Figure 1, in this section, the synthesis strategy will be discussed in the following four aspects: (1) mimicking the metal active sites of enzymes; (2) mimicking the substrate-binding pockets of enzymes; (3) mimicking the scaffolds/subunit of enzymes; (4) mimicking the allosteric regulation of enzymes.

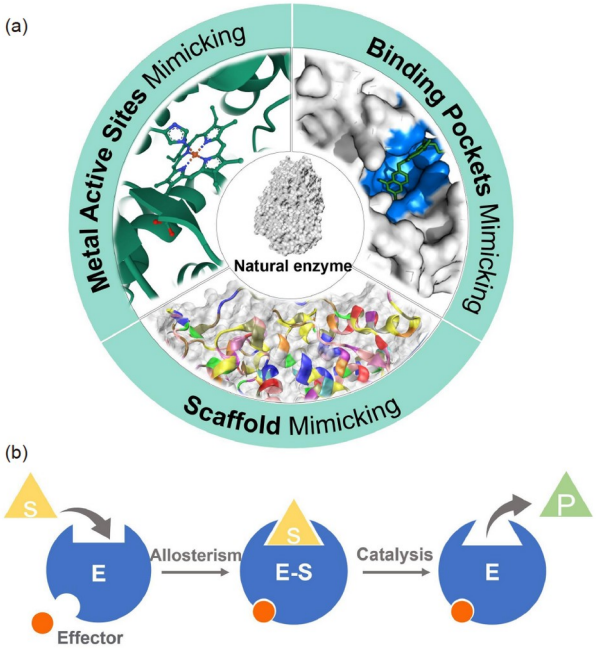

Figure 1 (a) Geometric structure of natural enzymes including metal active sites, binding pocket, and scaffold (PDB ref: 1ARP). (b) Schematic illustration of natural enzymes' allosteric regulation (color online).

2.1 Mimicking metal-active sites

In view of biology, the active site of the natural enzyme is defined as a region where substrate molecules proceed to a typical chemical reaction involving substrate conversion and have the ability to lower the activation energy significantly. It acts as the most critical component of the enzyme. To this end, the most efficient strategy to obtain comparable catalytic performance with natural enzymes is mimicking their active sites.

Recently, inspired by the architecture of natural enzyme active sites, respectable nanozymes have been reported to exhibit intriguing enzymatic performances with enzyme-like active sites. Most of them are metal-centered. Among them, nanozymes with oxidoreductase and hydrolase activities have been extensively reported. These nanozymes are analogous to metalloenzymes in nature. In fact, in biological evolution, metalloenzymes with various metal active sites play a vital role in aerobic catalysis, which constitutes a significant leap forward in the composition of the Earth's life form. And transition metals have been selected as "the chosen" metal to perform biological functions in metalloenzymes owing to (1) their larger radius to accommodate ligands, allowing the close proximity to isolated reactive sites and structural domains, (2) generally unfilled inner *d*-orbitals acting as an "electron sink" for versatile reactions, and (3) diverse coordination forms, variable coordination numbers, and regulable activity precisely adjusted by the surrounding ligands. The latest progress in mimicking metalloenzymes is divided into three typical transition metal active sites: iron-containing metalloenzymes, zinc-containing metalloenzymes, and copper-containing metalloenzymes. The central metal and coordination environments of these three representative metalloenzymes are shown in Figure 2, and the progress of nanozymes in mimicking these active sites is outlined in detail in the following section.

The abundance and multifunctionality of iron-containing metalloenzymes has attracted significant interest. As a representative iron-containing metalloenzyme, horseradish peroxidases (HRP) are robust enzymes that catalyze diverse substrates in the presence of H_2O_2, showing splendid applicability in biochemistry. Since the first discovery of Fe_3O_4 NPs to oxidize its substrate, HRP has aroused wide concern. Subsequently, plenty of nanozymes with Fe active sites have been developed to match the excellent catalytic performance of HRP. Among them, a remarkable work by Li and coworkers [55] developed a FeN_3P-centred single-atom nanozyme with an explicit electronic coordination environment. By simulating the atomically dispersed metal active center of the HRP enzyme, FeN_3P–SAzyme achieved comparable catalytic efficiency (k_{cat}/K_m=1.40×10^8 mol^{-1} L min^{-1}), resembling HRP (k_{cat}/K_m=1.15×10^7 mol^{-1} L min^{-1}) (Figure 3a). It was proved that the well-engineered Fe active site of

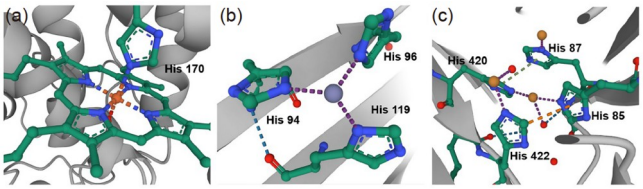

Figure 2 Active site structures of metalloenzymes. (a) Fe-containing metalloenzyme: horseradish peroxidase, (PDB: 1HCH). (b) Zn-containing metalloenzyme: human carbonic anhydrase II, comprising a tetrahedrally coordinated Zn^{2+} ion with three histidine imidazoles (PDB: 2CAB). (c) Cu-containing metalloenzyme: laccase (PDB: 1V10) (color online).

FeN_3P-SAzyme mimics the Fe active site of HRP, contributing to its extraordinary efficiency and selectivity. Furthermore, the precise introduction of P atom as the electron donor in the active site structure lowers the barriers to the formation of OH and O species by H_2O_2 dissociation. It thus leads to the improved affinity for the substrate as well as a higher POD-like catalytic performance by comparison of the Fe_3O_4 nanozyme, endowing the FeN_3P–SAzyme with a 30-fold enhancement in specific activity values (U mg^{-1}, Figure 3b). This work also provides an efficient therapeutic technique for preventing the proliferation of tumor cells *in vitro* and *in vivo*. Cytochrome P450 (CYP) is another type of iron-containing metalloenzyme that plays a pivotal role in drug metabolism. Our group [31] reported a Fe–N–C nanozyme with a heme-like Fe–N_x coordination active site that resembles CYP. Such feature not only enabled the Fe–N–C nanozyme with the ability to metabolize the cardiovascular drug but also demonstrated inhibition behaviors similar to CYP in accessing drug–drug interactions. Besides, cytochrome c oxidase (CcO) is the terminal oxidase in the respiratory electron transport chain of cells. It can transfer electrons from four cytochrome c molecules to oxygen, leading to the $4e^-$ reduction to water. In another elegant study, by embedding FeN_5 active sites into carbon nanoframe, 70 times higher OXD-like activity than commercial Pt/C was achieved [56]. The axial N-coordinated FeN_5 active site resembles the axial histidine (H376)-coordinated heme in natural CcO, resulting in its outstanding CcO-like performance in completing the electron transfer from cytochrome c molecules to O_2 [57].

As another earth-abundant metal, zinc stands out due to its unique full-filled *d*-orbital which allows it to serve solely as the Lewis acid. Zinc-containing metalloenzyme covers more than 300 enzymes across all classes of enzymes, especially hydrolases. Carbonic anhydrase (CA), a hydrolytic zinc metalloenzyme, is known as a powerful enzyme in nature which catalyzes the carbon dioxide hydrolysis. To mimic the spatial structure of the CA active sites, Dincă *et al.* [58] established an MOF featuring a metal node with an N_3–ZnOH coordination environment. The secondary building units of MFU–4*l*–(OH) are highly structural fidelity to CA active sites, contributing to a similar mechanism of CO_2

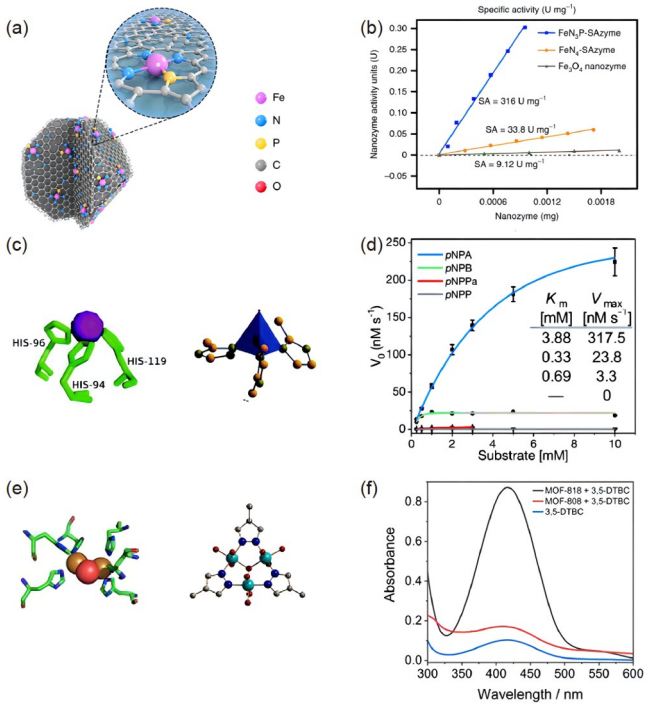

Figure 3 Mimicking metal active sites. (a) Model diagram of FeN_3P–SAzyme that mimics the active sites of a Fe-containing metalloenzyme horseradish peroxidase. (b) Comparison of FeN_3P–SAzyme, FeN_4–SAzyme, and Fe_3O_4 nanozyme's specific activities (nanozyme activity unit against their weight). (c) Model diagram of a ZIF-8 nanozyme that mimics the active sites of a Zn-containing metalloenzyme human carbonic anhydrase II. (d) Steady-state kinetic assay of ZIF-8 nanozyme in the presence of *p*NPA and other nitrophenyl esters with various concentrations. (e) Model diagram of the MOF-818 nanozyme containing trinuclear copper centers that mimic the active sites of a Cu-containing metalloenzyme catechol oxidase. (f) UV-vis absorption spectra of 3,5-di-*tert*-butylcatechol (3,5-DTBC, a catechol derivative) in the presence and absence of MOF-818 or MOF-808. (a, b) Adapted with permission from ref. [55]. Copyright 2021 Nature Publishing Group. (c, d) Reprinted with permission from ref. [59]. Copyright 2019 Royal Society of Chemistry. (e, f) Reprinted with permission from ref. [65]. Copyright 2020 American Chemical Society (color online).

hydration through inserting CO_2 into the Zn–OH bond. The coordination geometries of metal active sites are also crucial to their catalytic activity. In a complementary study, to mimic the coordination environment of CA active sites, Dong's group [59] fabricated a zeolitic imidazolate framework-8 (ZIF-8) nanozyme with hydratase-like catalytic performance, unraveling the specificity of ZIF-8 derived from the less 2-mIM-coordinated Zn^{2+} as enzyme-like molecular repeating units. This structure resembled the active center of human carbonic anhydrase II, comprising a tetrahedrally coordinated Zn^{2+} ion with three symmetric histidine imidazoles and one H_2O (Figure 3c). *p*-Nitrophenyl acetate (*p*NPA), a common chromogenic substrate frequently used to evaluate hydrolysis activity, was adopted to verify the excellent hydrolysis performance of ZIF-8 and its comparable affinity to *p*NPA analogous to CA (Figure 3d). Then, the CO_2 hydration ability of ZIF-8 was evaluated indirectly by ob-

serving the pH change. Due to the surface defects, ZIF-8 possesses Zn ions as Lewis acid sites, NH groups as Brønsted acid sites, and N-extremities as basic sites. H_2O and CO_2 tend to adsorb on the defect sites to form active Zn(2-mIM)$_n$O units (n=2, 3). The structural rationality of ZIF-8 as hydratase mimic has been well stated and the catalytic process of the natural CA has been illustrated as the decrease of the pK_a of H_2O molecules coordinated to the Lewis acid center of Zn^{2+}, which facilitates the formation of zinc-bound hydroxide ($Zn(His)_3OH$). Then the nucleophilic reaction between $Zn(His)_3OH$ and CO_2 yields HCO_3^-, finally leaving the active site. Besides these advances, more experimental proofs and theoretical calculations are still expected in future to unravel the working mechanism of hydrolase mimics.

Copper is widely distributed in nature and is active in biological processes because of its bioavailability and commonly accessible I/II redox pair. Laccase, a representative copper-containing metalloenzyme, possesses remarkable catalytic abilities and broad substrate specificity with four copper atoms in its active site. Liu's group [60] created guanosine monophosphate (GMP)-coordinated copper based on a MOF (denoted as Cu/GMP). The non-substitutability of Cu^{2+} as the central metal had been proven to be responsible for the laccase-like activity of Cu/GMP. Furthermore, inspired by the spatial coordination of the active site residues of laccase, He *et al*. [61] fabricated a CH–Cu nanozyme that mimicked the electron transfer site of Cu^+/Cu^{2+} coordinated with a Cys-His dipeptide. The as-prepared CH–Cu nanozyme is capable of oxidizing various phenolic substrates with a catalytic performance comparable to that of natural laccase. Similarly, Lu and coworkers [62] were also enlightened by the coordination microenvironment of the laccase active site, anchoring anions (Cl^-, Br^-) on the Cys–His bridge as a recognition antenna. The reaction rate and adsorption affinity towards 2,4-DP were significantly enhanced, therefore, providing a 150-fold improvement in the limit of detection for biomarker monitoring. Another example is natural catechol oxidase, a ubiquitous metalloenzyme containing binuclear copper metal centers coordinated to six histidine residues as the active site [63]. They play a crucial role in enzymatic browning by catalyzing the oxidation of catechol into corresponding *o*-quinones in the presence of oxygen to protect the damaged plant. Recently, a few nanozymes have been explored with ingenious catechol oxidase performance [64]. Among them, Dong's group [65] made an unprecedented work fabricating MOF-818 as catechol oxidase mimicking. MOF-818 was proved to contain trinuclear copper centers that mimic the active sites of natural catechol oxidase through SEM, TEM, XPS, XRD characterization (Figure 3e). 3,5-di-*tert*-butylcatechol (3,5-DTBC), a representative catechol oxidase substrate was utilized. The distinct absorption peak of 3,5-DTBC oxide at 415 nm displayed excellent catechol oxidase activity of MOF-818. Furthermore, the addition of 3,3′,5,5′-tetramethylbenzidine (TMB), a representative peroxidase substrate, or HRP alone cannot cause the TMB oxidation in the presence MOF-818, revealing that MOF-818 has high OXD-like specificity and no POD-like properties. In a contrast experiment, MOF-808 which only contains Zr metal with a similar octahedral structure was synthesized as a control, indicating the unsubstitutability of Cu as active sites (Figure 3f).

2.2 Mimicking binding pockets

The metal active sites give rise to the remarkable activity of enzymes, whereas the substrate-binding pockets of enzymes enable the binding/concentration and orientation of substrates, contributing to the specificity of natural enzymes. Indeed, the major challenge for nanozymes is their poor selectivity, presumably owing to the absence of substrate-binding pockets. In order to address this problem, pioneering work has contributed to the improvement of substrate selectivity through molecular imprinting by Liu's group [51]. On account of the poor selectivity of the classical peroxidase mimic Fe_3O_4 NPs towards various substrates, such as TMB and 2,2′-azino-*bis*(3-ethylbenzothiazoline-6-sulphonic acid) diammonium salt (ABTS), molecularly imprinted polymers (MIP) have been chosen for creating substrate-binding cavities on nanozymes to elevate selectivity. As shown in Figure 4a, TMB and ABTS were adsorbed onto Fe_3O_4 through electrostatic interactions. Upon the addition of monomers and cross-linker to the mixture, nanogels were formed, and binding pockets were created after washing away the substrate template, denoted as T-MIP and A-MIP respectively. According to the catalytic activity assessment, Fe_3O_4@T-MIP can specifically catalyze TMB rather than ABTS, whereas Fe_3O_4@A-MIP can specifically peroxidize ABTS over TMB (Figure 4b). Subsequently, based on the affinity between aminophenylboronic acid (APBA) and glucose, Zhang's group [66] coated the APBA-based MIP to AuNP, resulting in the high affinity and selectivity of AuNP nanozyme towards glucose. Further introducing oxygen-generating nanoemulsion boosted the catalytic efficiency by nearly 270-fold.

In addition to this molecular printing strategy to fabricate binding/recognition sites, substrate-binding pockets also feature conformational flexibility and thus can promote chemo-/stereo-selectivity and synergistic catalysis. Ma *et al*. [67] constructed a porous metalloporphyrin-based metal-organic aerogel, named Co-MMPG. Inspired by the enzyme's binding pocket with high conformational flexibility, in this contribution, porphyrin materials in gel form were verified to provide a high density of Lewis acid sites and the position of convergent binding sites allowed substrate molecules to be held in close proximity. Moreover, the two Co

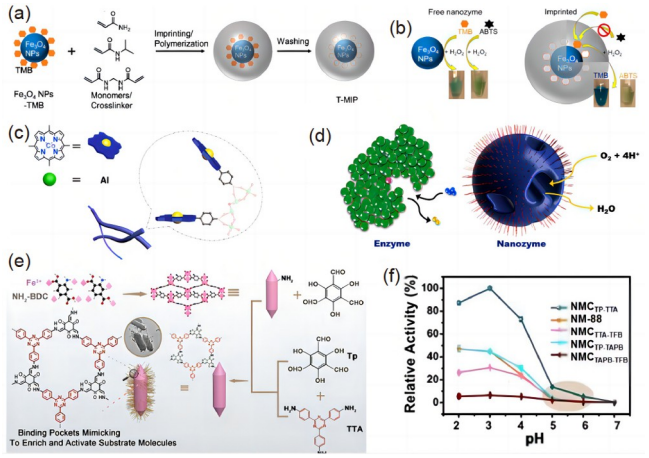

Figure 4 Mimicking substrate-binding pockets. (a) Schematic illustration of MIP-coated Fe_3O_4 nanozymes synthesis *via* the molecularly imprinted polymer strategy. (b) Schemes and photographs of free Fe_3O_4 and MIP-coated Fe_3O_4 nanozymes, indicating the activity and selectivity after creating substrate-binding pockets. (c) Model diagram of Co-MMPG local structure. The tetrahedrally coordinated Al species promote the flexibility and co-facial arrangement of the porphyrin rings by mimicking substrate-binding pockets. (d) Model diagram of PtNi nanozymes. Etching results in the formation of substrate channels, thus promoting the electrocatalytic performance. (e) Schematic illustration of NMC$_{Tp\text{-}TTA}$ nanozyme synthesis, the specific surface functional groups that mimic the binding pockets promote (f) the POD-like activity of NMC$_{Tp\text{-}TTA}$ nanozyme. (a, b) Reprinted with permission from ref. [51]. Copyright 2017 American Chemical Society. (c) Adapted with permission from ref. [67]. Copyright 2019 Nature Publishing Group. (d) Reprinted with permission from ref. [68]. Copyright 2018 American Chemical Society. (e, f) Adapted with permission from ref. [69]. Copyright 2020 John Wiley and Sons (color online).

(II) binding sites within the porphyrin-binding pocket promote synergistic catalysis (Figure 4c).

The creation of substrate-binding pockets can also elevate the activity of nanozymes by facilitating electron transfer and enriching substrate molecules. Gooding *et al*. [68] designed PtNi NPs with isolated, narrow channels by etching, which mimics the confined binding pockets of natural enzymes, leading to a 3.3-fold improvement in the electrocatalytic oxygen reduction reaction (Figure 4d). Recently, Qu and coworkers [69] made great progress in the creation of binding pockets on metal-organic frameworks (MOFs)-based nanozymes. By developing MOF as active sites and covalent organic frameworks (COFs) as binding pockets, the fabricated NMC$_{Tp\text{-}TTA}$ with hierarchical nanocavities formed a specific pore microenvironment that enriched and activated substrate molecules (TMB and H_2O_2) *via* noncovalent interactions (Figure 4e). This structure exhibited enhanced catalytic performance over a wide pH range (Figure 4f). Furthermore, the bacterial inhibition activity and therapeutic efficiency were proved to be amplified with the help of binding pockets. The author also suggested that the excellent antibacterial activity was attributed to the pseudopodia-like surface of the COF "skin" as binding pockets to capture bacteria and kill them by hydroxyl radicals generated *in situ*. This binding pocket structure offers weak basic surface functional groups that imitate the functions of amino-acid residues by forming hydrogen bonds with the substrate molecule.

2.3 Mimicking scaffolds

The scaffolds of natural enzymes are usually composed of biomolecular polymers, such as polypeptides. They play a vital role in providing a relatively confined environment, supporting the active sites, and offering a specific spatial organization. Since most nanozymes' backbones are inorganic nanomaterial with rigid structures, which are structurally different from the natural enzymes, the "scaffolding mimicking" strategy in this section refers to mimic the above three functionalities of natural enzymes. By learning from the scaffolds of enzymes, the processivity, stability, and substrate accessibility of nanozymes can be enhanced.

In order to create a relatively confined environment, MOFs are selected as promising scaffolds, because they are crystalline entities that consist of repeating building blocks. This feature endows them with well-defined coordination networks, highly ordered and tailorable cavities and channels, which provide a hydrophobic, confined environment. For example, Zhao's group [70] developed an outstanding one-step self-assembly strategy using $Mn_3[Co(CN)_6]_2$ as a scaffold loading single-atom Ru as the catalytically active site (Figure 5a). The O_{xge}MCC-r nanozyme exhibit rapid endogenous H_2O_2 decomposition and intracellular oxygen production ability, the enhanced POD activity was confirmed under hypoxic condition (Figure 5b). Furthermore, the high loading capacity of the Ce6 photosensitizer encapsulated in the MOF-based scaffold renders it a promising anticancer theranostic agent.

For supporting the active sites, metal nanoparticles are found to be a solution. For example, in bioorthogonal nanozymes, the incorporation of transition-metal catalysts into metal nanoparticles renders them with enhanced stability. The metal nanoparticles provide a solid support for the active sites, simulating the second function of the natural enzymes' scaffolds. Besides, recently, Rotello and co-workers [71] open up a new avenue where nanoparticle-based scaffolds can also actively participate in catalysis as a cofactor and accelerate the chemical transformation that cannot be accomplished by natural enzymes. This work reported a bioorthogonal nanozyme using ZnS nanoparticles as a biodegradable and biocompatible scaffold, the encapsulation of [Cp*Ru(cod)Cl] inside the nanozyme monolayer, and ligand-mediated acceleration of catalysis, resulting in the activation of a chemotherapeutic drug (Figure 5c). Prominently, the degradation process of ZnS scaffolds enhanced the catalytic performance in solution and in cells by the release of thiolate surface ligands, thus providing an efficient mode to kill cancer cells (Figure 5d).

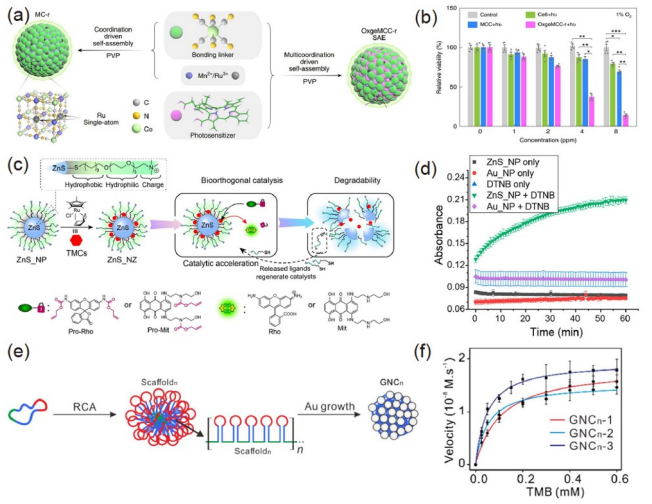

Figure 5 Mimicking scaffolds. (a) Schematic illustration of the synthesis of MOF-based O_{xge}MCC-r nanozymes. (b) Cell viability assay in the presence of O_{xge}MCC-r nanozyme and 671 nm light irradiation under hypoxic conditions. (c) Schematic illustration of the synthesis of a bioorthogonal nanozyme using ZnS nanoparticles as scaffolds. (d) The increasing UV-vis absorbance of Ellman's reagent (DTNB) at 412 nm indicates the degradation of the ZnS scaffold. (e) Schematic illustration of the synthesis of GNC_n nanozymes using ssDNA as a scaffold. (f) Michaelis–Menten curves of GNC_n nanozymes using TMB/H_2O_2 as substrates. (a, b) Adapted with permission from ref. [70]. Copyright 2020 Nature Publishing Group. (c, d) Reprinted with permission from ref. [71]. Copyright 2022 American Chemical Society. (e, f) Reprinted with permission from ref. [72]. Copyright 2022 American Chemical Society (color online).

DNA nanostructure has emerged as a potential scaffold due to its high-precision encodability. It can organize functionalized nanoparticles to provide programmable spatial organization, which is analogous to the third function of the natural enzymes' scaffolds. Very recently, Li and co-workers [72] reported admirable work on engineering the spatial organization of gold nanoparticle clusters (GNCs) using ssDNA as scaffolds, and polyA loops as specific sites for controlled growth of GNCs, which is inspired by the spatial organization of biopolymer scaffolds in nature. Moreover, polymeric GNCs with self-folding ssDNA as scaffolds possess POD-like catalytic activity, which can be fine-tuned by adjusting the size and inter-polyA sequence length of the scaffold (Figure 5e). GNC_n-3 (*n* denotes clusters with multiple particles) was proven to exhibit superior catalytic activity with the highest substrate affinity owing to the high density of catalytic units, sufficient interspace for reactant exchange that promotes the catalysis, and moderate interparticle fusion structures (the abundance of accessible catalytic surfaces with minimal surface capping) (Figure 5f).

2.4 Mimicking allosteric regulation

An admirable biomimetic control mechanism that imitates the allosteric regulation of enzymes was reported by Rotello *et al.* [73] in 2015. The construction of allosteric nanozymes was based on the bioorthogonal model reaction of ruthenium-catalyzed deallylation, and biomimetic sized AuNPs was used as a scaffold to support Ru-catalyst (Figure 6a). First, benzyl-ligand-protected gold nanoparticles were successfully synthesized by the Brust–Schiffrin two-phase synthesis method and confirmed by mass spectroscopy (denoted as NP, Figure 6b). Then, NP_Ru was fabricated by immobilizing [Cp*Ru(cod)Cl] catalyst (Cp*=pentamethylcyclopentadienyl, cod=1,5-cyclooctadiene) into the hydrophobic portion of the AuNP. The encapsulation of catalysts was proved by transmission electron microscopy (TEM) and dynamic light scattering, and no aggregation and size change were observed (Figure 6c), indicating no morphological change after the encapsulation. The NP_Ru nanozyme could drive the allylcarbamate cleavage of the substrate of *bis*-*N*,*N*'-allyloxycarbonyl rhodamine 110 efficiently, yielding bright fluorescence. Next, cucurbit[7]uril (CB[7]) was introduced as a reversible regulating component due to its complexation of the benzyl headgroup of the NP. Isothermal titration calorimetry measurement was performed to reflect the heat changes during the complex formation, and the fitted binding isotherm curve indicated the successful fabrication of NP_Ru_CB[7] (Figure 6d). The catalytic activity of the NP_Ru_CB[7] was heavily shielded as shown in Figure 6e. However, it was completely recovered after the addition of 1-adamantylamine (ADA) as a competitive guest molecule (Figure 6f). Through the delicate reversible activity control achieved by the host–guest interaction, this bioorthogonal nanozyme worked efficiently in the living cells, endowing nanozymes with promising therapeutic and imaging applications that are inaccessible by means of natural enzymatic processes.

In order to realize reversible control and temporal–spatial resolution without extra molecule addition, Qu's group [54] made contributions to a light-controlled bioorthogonal nanozyme using the reversible interaction between azobenzene and cyclodextrin (CD). As illustrated in Figure 6g, macroporous silica nanoparticles (DMSN) were used as a scaffold to stabilize the Pd^0-based catalyst. By coordinating and electrostatic interaction, SP was synthesized and the formation of Pd NPs on silica was proved by powder X-ray diffraction (XRD) (Figure 6h), which was consistent with the SEM-EDX, TEM, XPS, and elemental mapping results. The resulting SP exhibited the high efficiency on the allylcarbamate cleavage of N-allyloxycarbonyl coumarin. Then, ASP was prepared by conjugating an azobenzene switch on the surface of SP with the verification of XPS and Fourier transformation infrared spectroscopy (FTIR) spectra. Next, CD was selected as the gatekeeper owning to its combination with azobenzene. As the FTIR spectrum in Figure 6i suggested, the decreased band at 1,540 cm^{-1} and 640 cm^{-1} was ascribed to the interaction between CD and azobenzene, supporting the successful fabrication of CASP. The func-

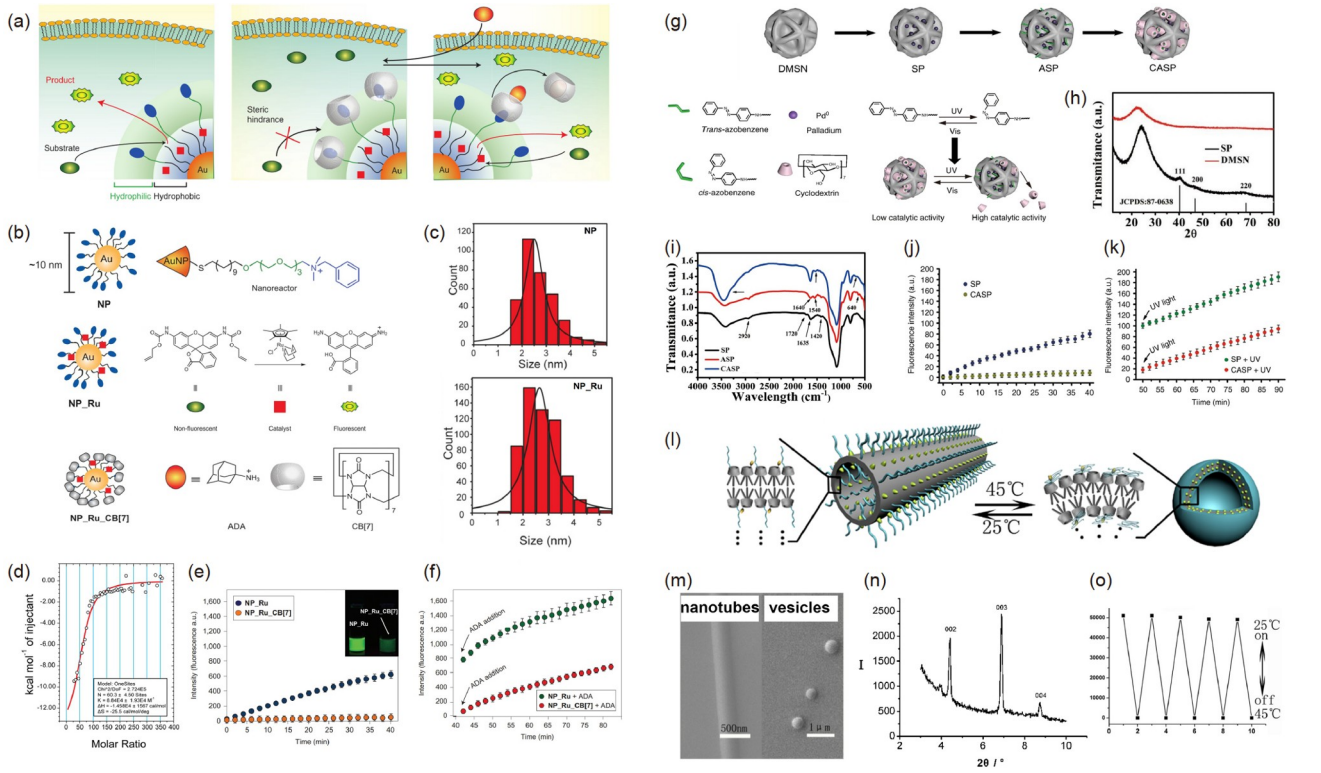

Figure 6 Mimicking allosteric regulation. (a) Schematic illustration of the bioorthogonal allosteric nanozyme design. (b) Schematic illustration of the structure of AuNP, NP_Ru, and NP_Ru_CB[7] bioorthogonal nanozymes. (c) Dynamic light scattering of NP and NP_Ru. (d) Isothermal titration calorimetry curve of CB[7]s into the NP solution. (e) The catalytic activity of nanozymes. NP_Ru exhibits strong fluorescence following profluorophore cleavage, whereas NP_Ru_CB[7] exhibits no notable change. (f) Addition of ADA restored the catalytic activity of NP_Ru_CB[7], while the performance of NP_Ru remained unchanged. (g) Schematic illustration of intracellular azobenzene isomerization by UV light activation, imitating the allosteric regulation of enzymes and the structural formulae of *trans*-azobenzene, *cis*-azobenzene, palladium, and cyclodextrin. (h) The XRD patterns of SP and DMSN. (i) The FTIR spectra of the SP, ASP and CASP. (j) The catalytic activity of the SP nanozyme revealed strong fluorescence, whereas the CASP nanozyme revealed inhibited fluorescence. (k) After UV light irradiation, the fluorescence of CASP was restored, while that of SP remained unchanged. (l) Schematic illustration of the temperature-driven shape transformation from nanotubes to vesicles. (m) SEM images indicate a reversible transition from the tube to the vesicle. (n) XRD patterns of the nanotubes. (o) On–off POD-like activity *via* the reversible nanostructure transformation from tube to vesicle. (a–f) Reprinted with permission from ref. [73]. Copyright 2015 Nature Publishing Group. (g–k) Adapted with permission from ref. [54]. Copyright 2018 Nature Publishing Group. (l–o) Reprinted with permission from ref. [74]. Copyright 2014 American Chemical Society (color online).

tionalization of ASP with CD blocked the catalytic site of the ASP, leading to inhibited catalytic activity of CASP (Figure 6j). The light-induced activity regulation was achieved by the isomerization of azobenzene under UV stimuli, which allowed the release of the CD blocker from the catalysts resulting in restored catalytic activity (Figure 6k). By using the reversible interaction between azobenzene and CD with low-dose light as the external stimulus, the light-controlled nanozyme was successfully explored with precise locations and artificially adjustable catalytic activity to maintain homeostasis for long-term therapies.

Another interesting work was reported by Liu *et al.* [74] Based on host–guest chemistry, cyclodextrin was also used as the host molecule, whereas the thermosensitive polymer and catalytic core of glutathione peroxidase functioned as guest molecules (Figure 6l). Using temperature as a switch trigger, the reversible transformation of the as-prepared nanozyme from the tube-like to sphere-like structure was observed *via* SEM (Figure 6m), and the tubular structure was confirmed by XRD (Figure 6n). Interestingly, The ON–OFF switches for peroxidase activity were accomplished by simply adjusting the temperature (Figure 6o).

The above-mentioned biomimetic structural designs provide strong evidences of significantly improved activity and selectivity of nanozymes. But just like "too much water drowned the miller", redundant biomimicking may pose a threat to the stability, along with the higher manufacturing cost. Therefore, the rational design of nanozymes also needs to find a balance between performance, engineered structure, and cost.

3 Molecular-scale elucidation of nanozymec mechanism

3.1 Overview of nanozymes' catalytic mechanism

Understanding the reaction mechanism is essential for the rational design of nanozymes with an explicit structure-

activity relationship. Generally, the catalytic mechanism of most nanozymes consists of (1) the electron transfer pathway and (2) the reactive-species-induced pathway. In the electron transfer pathway, nanozymes are capable of transferring electrons from biomolecules to O_2/H_2O_2. In this case, biomolecules function as electron donors and O_2/H_2O_2 as electron acceptors. The versatility of the nanozyme surface stimulates the electron exchange between the substrate and O_2/H_2O_2, thus leading to the oxidation of substrates as well as the reduction of O_2/H_2O_2 [75,76] (Figure 7a).

In the latter situation, the reactive-species-induced pathway can further be classified into two categories: (1) the free ROS pathway (ROS represents reaction oxygen species, typically, H_2O_2, $^1O_2$, $^{\bullet}OH$, and $O_2^{\bullet-}$); among them, $^{\bullet}OH$ is regarded as the most powerful species generated by the Fenton reaction or Haber–Weiss reactions; (2) the bound ROS pathway, such as metal–oxygen intermediates (M-oxo, M-peroxo, M-superoxo, M-hydroperoxo species, and high-valent metal–oxygen species). These metal–oxygen species have attracted much attention in the dioxygen activation and oxidation reactions, resembling the key intermediates in the catalytic cycle of natural enzymes [77]. From a viewpoint of kinetic mechanism, taking the representative POD process for example, the free ROS pathway allows one molecule of H_2O_2 to react with POD nanozymes to form $^{\bullet}OH$, and the formed $^{\bullet}OH$ would abstract H^+ from biomolecule substrates

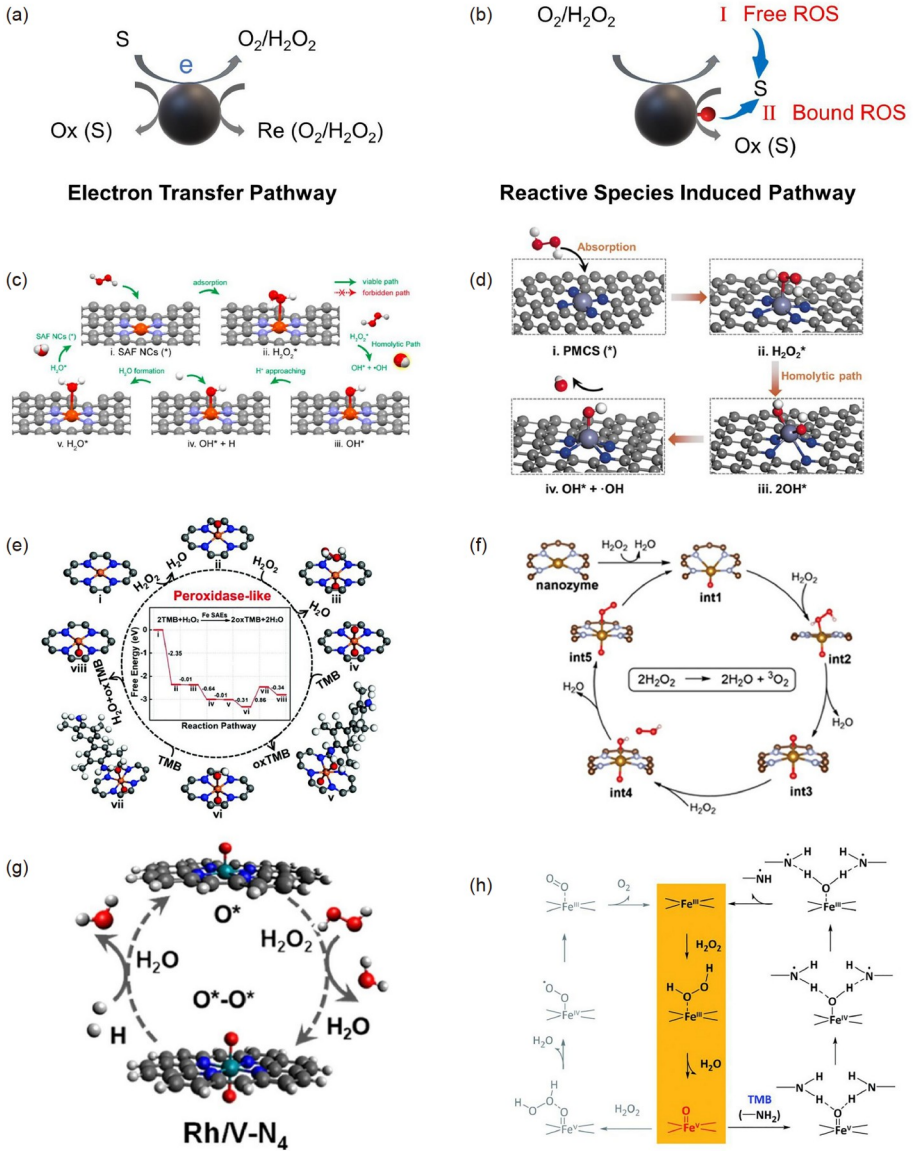

Figure 7 Catalytic mechanism of nanozymes. (a) Electron transfer pathway of nanozymes. (b) Reactive species-induced pathway of nanozymes, which includes (c, d) free-ROS pathway and (e–h) bound-ROS pathway. (c) Reprinted with permission from ref. [81]. Copyright 2019 American Chemical Society. (d) Reprinted with permission from ref. [82]. Copyright 2019 John Wiley and Sons. (e) Reprinted with permission from ref. [79]. Copyright 2019 Royal Society of Chemistry. (f) Reprinted with permission from ref. [83]. Copyright 2022 John Wiley and Sons. (g) Reprinted with permission from ref. [50]. Copyright 2022 Nature Publishing Group. (h) Reprinted with permission from ref. [84]. Copyright 2021 Royal Society of Chemistry (color online).

as the hydrogen donor further accomplishing the substrate oxidation [1,78]. The bound ROS pathway allows one molecule of H_2O_2 combining with POD nanozymes to generate an M–O intermediate, and then the generated intermediate would abstract H^+ from biomolecule substrates as the hydrogen donor further accomplishing the catalytic peroxidase process [22,79,80]. The difference between the free ROS pathway and the bound ROS pathway relies on whether the biomolecule substrate reacts with the nanozyme.

Generally, the structural inhomogeneity of nanozymes makes it difficult to determine the true geometries of the active sites thus hindering the catalytic mechanism of nanozymes. Single-atom nanozymes with atomically dispersed metal active sites and maximum efficiency of utilizing atoms have become a highly active frontier in the catalysis field, the appearance of single-atom systems makes single atom nanozymes (SAzymes) an ideal platform for the exploration of the catalytic mechanism with the cooperation of theoretical simulations and experimental works. Therefore, SAzymes were chosen as models in this section. Asterisks (*) represent the species adsorbed on the nanozyme surface.

Figure 7c and d demonstrate the general routine of the free ROS pathway producing $^{\bullet}OH$ species [81,82]. The $^{\bullet}OH$ species in this pathway were first observed by trapping agent *via* spectrograph or electronic spin resonance. The possible catalytic mechanism can be further unraveled in combination with theoretical calculations, which include the adsorption of H_2O_2 molecule on the M–N_4 active sites (i). The homolytic dissociation of activated H_2O_2 molecule into two OH species ($^{\bullet}OH$+OH* or OH*+OH*) (ii). Then, the desorption of OH* led to the generation of $^{\bullet}OH$ species (iii).

Due to the similarity between bound ROS and other oxidation species, the bound ROS is difficult to be directly identified experimentally at the current stage. Thus, theoretical calculations help shed light on the identification of bound ROS. Figure 7e–h depicts several routines that represent the bound ROS pathway. In the case of the Fe–SAzyme with superior POD-like activity, the O=Fe=O intermediate was proven to be favorable for the activation of the TMB molecule [79]. As shown in Figure 7e, the H_2O_2 molecule was first adsorbed on the Fe–N_4 active sites. The O–O cleavage of H_2O_2 led to the formation of an Fe=O intermediate and H_2O. Then, the O=Fe=O intermediate was formed by the heterolytic dissociation of another H_2O_2 molecule on the other side of the central Fe–N_4. The active O=Fe=O intermediate is responsible for the activation of the first TMB molecule by forming an O–H bond, contributing to the H atom abstraction from TMB molecule to generate oxTMB and O=Fe–OH. This structure is favorable to extract another H atom from another TMB molecule to form another oxTMB and H_2O, which is the rate-determining step.

In addition to dominating the POD-like activity, the M–O species contributes to the CAT-like process [83]. An Fe–N_4–SAzyme with boosted CAT-like performance was developed, and the reaction process was proposed to begin with the generation of a pentacoordinate Fe–O intermediate, which is the real active part for the conversion of H_2O_2 into H_2O and $^3O_2$ (Figure 7f).

The significance of the M–O species is not limited to non-noble metal SAzyme reactions. In another elegant study, the M–O active species was also proven to be responsible for the high catalytic efficiency of Rh–N_4 and V–N_4 SAzymes [50]. The stable attachment of the O atom lowers the ionization of the metallic atom, resulting in more effective decomposition of the H_2O_2 molecule. The proposed catalytic mechanism follows a two-sided oxygen-linked pathway (Figure 7g). The catalytic process begins with H_2O_2 molecules adsorbed onto the active sites of the SAzymes. Then, the M–O intermediate was yielded by releasing an H_2O, and such a state is favorable for the bilateral adsorption on the other side; thus, another H_2O_2 molecule is feasible to be captured to generate a two-sided oxygen-linked intermediate and release another H_2O molecule.

Notably, the indistinguishability of the free ROS pathway is generally robust while hinders the specificity of nanozyme. The bound ROS pathway was disclosed as the origin of the intrinsic selectivity of Fe/CoN_x SAzymes through a bound oxygen-atom transfer process [84]. Briefly, H_2O_2 was coupled to N-coordinated Fe^{III} in Fe–N–C to generate Fe^{III}-superoxo species, and the oxidation of Fe^{III} to Fe^{V}=O is followed by the O–O cleavage of H_2O_2 to release a water molecule. The Fe^{V}=O active species play a key role in the selective oxidation of the substrate, depending on the affinity between Fe^{V}=O and the substrate molecule (Figure 7h). In addition to the single-atom nanozyme model, an up-to-date advance suggests that such high-valent Fe=O active species are also responsible for the POD-like activity of Fe_3O_4 nanoparticles [85].

3.2 Overview of nanozymes' kinetic mechanism

From the perspective of kinetics, since the nanozymatic reactions follow the typical Michaelis–Menten kinetic model and most of them are eligible for the double substrate characterization. Currently, a handful nanozymes have unveiled the consistency with enzymes' multi-substrate kinetic mechanism, disclosing the binding order of multiple substrates. This mechanism can be divided into ping-pong or sequential types. For the former, one substrate first binds to the nanozyme, followed by releasing the first product, and then the second substrate binds and reacts. For the latter, two substrates bind to the nanozyme before releasing the first and second products with the random or ordered sequence. For example, in the investigation of Fe_3O_4 MNPs as POD mimics, by using the Lineweaver–Burk plot, the parallel slope of lines was observed, indicating the typical characteristic of

a ping-pong mechanism [1]. Additionally, GeO_2 nanozymes were reported to follow the sequential Bi–Bi mechanism, owning to the observation of intersected lines in the Lineweaver–Burk plot [86].

3.3 Overview of typical nanozymes' catalytic pathways

Generally, different nanozyme reactions follow various reaction pathways *via* diverse intermediates. To rationally design nanozymes with specific activities at a molecular level, both mechanisms and intermediates under working conditions should all be taken into deliberate consideration. As oxidoreductase-like nanozymes account for 96.1% of all nanozymes, four typical nanozyme reactions regarding oxidoreductase are mentioned in this section, which focus on the intermediates. (Figure 8)

3.3.1 OXD-like activity

The main mechanism of nanozymes with OXD-like activity arises from the dissociation of O_2 into H_2O or H_2O_2, where the $4e^-$ oxidase-mimic process could be initiated upon the adsorption of an O_2 molecule with a more energetically favorable O_2 adsorption configurations. (Side-on or end-on manner) (i). O_2 dissociates into two chemically adsorbed O* (ii). O* abstracts hydrogen either from the solvent or substrate to generate H_2O* species or to oxidize the substrate owing to its Brønsted-base character (iii). Then, the H_2O* desorbs from the nanozyme surface (iv) [80,87].

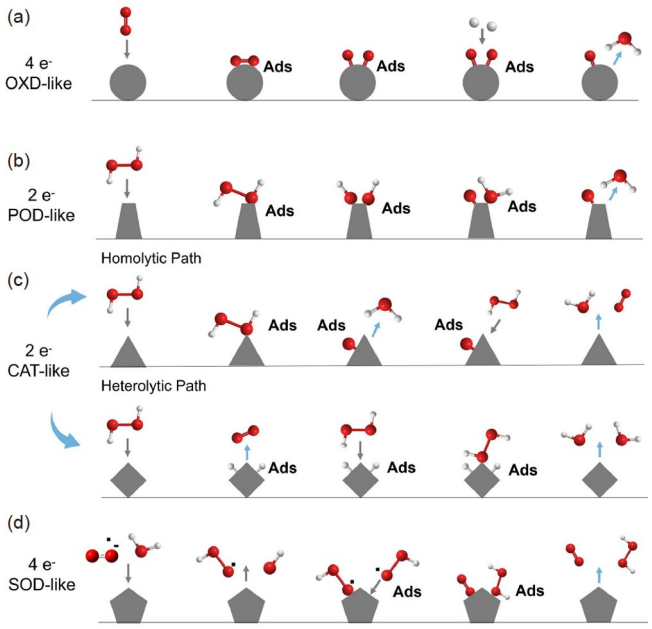

Figure 8 Typical catalytic pathways of nanozymes and adsorbed intermediates in four types of nanozyme reactions. (a) $4e^-$ OXD-like process, transferring O_2 into H_2O, (b) $2e^-$ POD-like process, transferring H_2O_2 into H_2O, (c) $2e^-$ CAT-like process, transferring H_2O_2 into O_2 and 2 H_2O and (d) $4e^-$ SOD-like process, transferring $O_2^{\bullet-}$ into O_2 and H_2O_2. Ads represents the species adsorbed on the nanozyme surface. The various shapes represent diverse types of nanozymes that undergo different catalytic pathways. Note that this is NOT the only catalytic pathway for a specific reaction, and we just give a typical example (color online).

A representative work on Au nanoparticles using glucose as the substrate revealed a $2e^-$ oxidase routine involving the reduction of O_2 to H_2O_2 [2]. It has been confirmed that the excellent OXD-like activity of Au NPs arises from the direct dehydrogenation of glucose with the highest affinity for lowering the breaking energy of the C–H bond and the electron transfer to O_2 as an electron acceptor. The higher energy barrier for breaking the O=O double bond contributes to the $2e^-$ routine to produce H_2O_2, while other noble metals Pt, Pd, Ru, Rh, and Ir NPs prefer to further continue the $2e^-$ routine to convert H_2O_2 to H_2O.

3.3.2 POD-like activity

As the most developed nanozyme, a POD-like nanozyme with a $2e^-$ POD-like mechanism takes lion's share of the nanozyme mechanism. The main mechanism of nanozymes with POD-like activity arises from the dissociation of H_2O_2, where the different microstructure and reaction conditions of nanozyme account for the multi-manners of H_2O_2 dissociation. Metal nanozymes have been reported to exhibit base-like decomposition of H_2O_2 under acidic conditions [88]. Specifically, the $2e^-$ POD-like process was initiated by H_2O_2 adsorption with proper adsorption energy according to the Sabatier principle. In this case, the adsorption of H_2O_2 on the nanozyme surface was thermodynamically more favorable than that of H_2O (i). Subsequently, H_2O_2* dissociated into two OH* species (ii). The rearrangement between the two OH* species generated an O* species and H_2O* molecule (iii). Then, H_2O* was desorbed from the nanozyme surface (iv).

3.3.3 CAT-like activity

An explicit mechanism of $2e^-$ CAT-like activity was presented based on the Fe–N–C nanozyme through the homolytic pathway [83]. First, a penta-coordinated intermediate was formed in the presence of H_2O_2, and adsorbed a H_2O_2 molecule with the strong binding interaction (i). Then, the O–O bond in H_2O_2* was broken, leading to the release of a H_2O molecule, which accounts for the rate-determining step (ii). Next, the second H_2O_2 molecule arrived (iii), and promoted the rearrangement of a H_2O molecule and a O_2 molecule (iv).

Another hypothetical mechanism of $2e^-$ CAT-like activity was proposed based on the CeO_2 nanozyme through a heterolytic pathway [89]. First, an H_2O_2 molecule was adsorbed on a suitable surface of nanozymes (i). H_2O_2* was then easily oxidized to O_2, which is exoenergetic and has a low energy barrier, giving rise to 2 H* (ii). Next, 2 H* promoted the adsorption of another H_2O_2 molecule (iii). Finally, 2 H_2O were rearranged and released from the nanozyme surface (iv).

3.3.4 SOD-like activity

Reportedly, a proposed mechanism of metal-based nanozymes with SOD-like activity was initiated at the protonation of $O_2^{\bullet-}$ *via* a reversible reaction in which $O_2^{\bullet-}$ acted as a Brønsted base [80,89] ($O_2^{\bullet-}+H_2O_2 \rightleftharpoons HOO^{\bullet}+OH^-$) (i). Then, $HOO^{\bullet}$* was chemisorbed and rearranged at the proper positions on the nanozyme surface with the strongest adsorption energies (ii). Next, the chemisorption of another $HOO^{\bullet}$* resulted in the generation of O_2* and H_2O_2* owning to the favorable thermodynamics process (iii). Finally, O_2* and H_2O_2* were desorbed into O_2 and H_2O_2 molecules (iv).

The above catalytic pathways present typical nanozyme pathways covering key adsorbed intermediates with specific nanozyme model. It should be noted that, currently, more than 1000 nanozymes have been developed with a rich toolbox of metallic, metal oxides, carbon-based nanomaterials, metal-organic frameworks, and so on. For different types of nanozymes with similar activities, the form in which the O_2, H_2O_2, $O_2^{\bullet-}$ molecules adsorb to the nanozyme surface, break, and rearrange, as well as undergo their intermediate states is closely associated with their nanostructures. In these regards, factors such as composition, morphology, surface modification, and active site structure related to the nanostructure should be taken into consideration [37]. Moreover, for example, in natural enzyme catalysis, the peroxidase and catalase share the same active heme structure while have completely different pathways to activate H_2O_2 mainly due to their different microenvironments. Similarly, even for similar types of nanozymes, the surface properties, the coordination environment of the active sites, and even the working conditions [88] should be taken into deliberate consideration concerning the catalytic pathway.

3.4 Descriptors

With the rapid development of high-throughput computations, the performance trends of a series of nanozymes can be described using proper descriptors on the basis of understanding the important intermediates and catalytic processes of nanozymes.

3.4.1 Electronic structure descriptors

A descriptor can be used to describe the activity of nanozymes. Nanozyme reactions involve several important surface intermediates that are crucial for enzyme-like activities. Based on the observation of the strong correlation between activation energies for elementary surface reactions and adsorption energies, volcano relations between interaction strength and adsorption energies of important intermediates adsorption energies (E_{ads}), and dissociative chemisorption energy (E_{diss}), have been widely identified in heterogeneous catalysis according to the Sabatier principle [90].

Gao's group [91] represents a significant advance in predicting peroxidase mimics and unveiling quantitative structure–activity relationships. The H_2O_2 chemisorption energy ($E_{r,1}$) was proposed to predict the POD-like activity of the iron-oxide-based nanozyme surface and indicated a remarkable POD activity when $E_{r,1}$ varied in the energy window ranging from −3.6 to −0.3 eV (Figure 9a). In addition, the adsorption energy of hydroxyl radical of $^{\bullet}OH$ ($E_{ads,\ OH}$) was proven to have a good linear relationship with $E_{r,1}$. Thus, $E_{ads,\ OH}$ can also be an effective and simple descriptor. This work also suggested a boost POD-like activity when $E_{ads,\ OH}$ varied in the energy window ranging from −3.6 to −1.6 eV. It was predicted that the POD-like performance would achieve the optimal value when $E_{ads,\ OH}$=2.6 eV (Figure 9c). The applicability of $E_{ads,\ OH}$ as an activity descriptor was identified for various nanomaterials presented in Figure 9d.

As the classic descriptor, the *d*-band model was established for the first time in 2009 by Nørskov [92] to evaluate the relative reactivity of a series of transition metals. According to the *d*-band center theory, the higher in energy of the metal's *d*-states compared with the Fermi level, the higher the energy of the metal's antibonding states, and hence the stronger the metal's reactivity. In another elegant study, the *d*-band center was applied to evaluate the OXD-like activity of Pd, Pt, Au, and Ag nanozymes with (111) facets [80]. DFT calculations showed that their *d*-band centers were −1.8, −2.4, −3.5, −4.1, respectively, which agreed well with the predicted activity order Pd (111)>Pt (111)>Au (111), Ag (111). This work suggests the applicability of the *d*-band center as a descriptor of the OXD-like activity of metal-based nanozymes.

e_g occupancy has been successfully studied as an appropriate descriptor for electro-catalysts. Wei's group [93] made provoking work on the establishment of the activity descriptors for designing enzyme-mimicking nanocatalysts. A volcano relationship between the e_g occupancy and the specific POD-like catalytic activity of ABO 3-type perovskite transition-metal oxides was identified. DFT calculations were performed to investigate the catalytic mechanism of the (001) facet of ABO_3 as peroxidase mimics. The variations in the adsorption energies (E_{ads}) for O ($E_{ads,\ O}$) and OH ($E_{ads,\ OH}$) with the e_g occupancy also revealed a volcano-like relationship. Specifically, when the e_g occupancy was approximately 1.2, the weakest O and OH adsorption was observed, indicating the highest accessibility of oxygen species to the TMB substrates and thus contributing to the highest peroxidase-mimicking activity. e_g occupancies lower or higher than 1.2 give rise to stronger adsorption energies. Meanwhile, the rate-determining step of the former relied on the oxidation of the substrate, and the latter could be ascribed to the O–O bond splitting of the adsorbed H_2O_2*. The general applicability of e_g occupancy has proven to be effective. This work paved the way for the e_g occupancy as the descriptor to predict the enzyme-like activities of other metal oxides (Figure 9b).

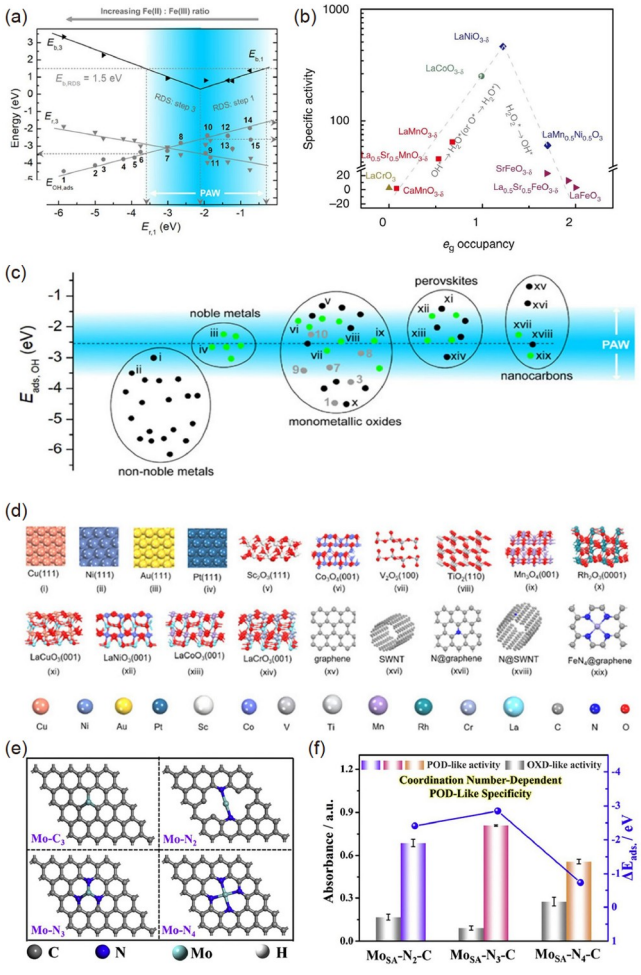

Figure 9 Descriptors of nanozyme activity regarding the electronic structure and geometric structure. (a) The blank lines show the POD-like activity of iron-oxide-based nanozymes plotted as a function of H_2O_2 chemisorption energy ($E_{r,1}$). The gray lines show $E_{r,3}$, and $E_{ads, OH}$ plotted as a linear function of $E_{r,1}$, and the blue zone shows the decreasing POD-like activity from blue to white defined by $E_{r,1}$. (c) Overview of the POD-like activities of various nanozymes. The blue zone shows the decreasing POD-like activity from blue to white defined by the hydroxyl adsorption energy ($E_{ads, OH}$). (d) The structures of various nanozymes corresponding to (c). (b) The volcano-shaped plot of the POD-like activities of perovskite TMOs plotted as a function of e_g occupancy (e) Model diagram of optimized Mo–C_3/N_x structures in Mo$_{SA}$–N_x–C nanozyme, x=2,3,4. (f) The enzyme-like activities of Mo$_{SA}$–N_x–C nanozymes and the difference value between H_2O_2 and O_2 adsorption energies. (a, c, d) reprinted with permission from ref. [91]. Copyright 2020 American Chemical Society. (b) reprinted with permission from ref. [93]. Copyright 2019 Nature Publishing Group. (e, f) reprinted with permission from ref. [94]. Copyright 2020 Elsevier Inc (color online).

3.4.2 Geometric structure descriptors

Except for electronic structure factors, the trends and descriptors of nanozyme activity have been explored extensively with respect to the geometric structure, namely, coordination number, bond length, and oxidation state. Meanwhile, the rapid development of fine structure characterization and theoretical computations has shed light on the confirmation of the detailed structure of nanozymes.

Zheng and coworkers [94] reported a rational design on a series of heterogeneous molybdenum nanozymes (Mo$_{SA}$–N_x–C). In order to gain further insight into the dominant enzyme-like properties, the difference in adsorption energy (ΔE_{ads}) between O_2 and H_2O_2 molecules was taken as a convenient descriptor, The three-nitrogen-coordinated Mo exhibited the most specific POD-like performance with a more negative ΔE_{ads}. Furthermore, Mo$_{SA}$–N_x–C with different Mo–N_x coordination numbers (x=2, 3, 4) were obtained under different pyrolysis treatments and confirmed *via* X-ray absorption spectroscopy (XAS) and X-ray photoelectron spectroscopy (XPS) (Figure 9e). Through the manipulation of Mo–N_x coordination numbers, a direct correlation was successfully established between the POD-like specificity and configurations of Mo$_{SA}$–N_x–C nanozymes (Figure 9f), indicating the coordination number and ΔE_{ads} as the instructive descriptors for POD-like specificity.

4 Emerging methodologies for activity assessment

The universal activity assessment methods of nanozymes are generally related to detection probes and platforms. The OXD-like and POD-like activities have been evaluated by various enzyme substrates, such as TMB, ABTS, di-azo-aminobenzene (DAB) and *o*-phenylenediamine (OPD). Likewise, different probes have been applied to evaluate the SOD-like activity, such as nitro-blue-tetrazolium (NBT), iodonitrotetrazolium chloride (INT), water-soluble tetrazolium salt (WST)-8 and 5,5-dimethyl-1-pyrroline-N-oxide (DMPO). The CAT-like activity has been evaluated using the dissolved oxygen sensor, spectrophotometric assay, electron paramagnetic resonance and so on. The strengths and weaknesses of various probes and the applicable scope of these methods have been comprehensively studied in previous reports [95,96].

From a kinetic viewpoint, the activity assessment principle of nanozymes using the Michaelis–Menten kinetic model was first proposed, owing to the remarkable performance of nanozymes in catalyzing the substrates of enzymes under mild conditions. However, on account of the distinctiveness of nanozymes in reaction mechanisms and catalyst separation, turnover frequency is also proposed to assess nanozyme activity resembling heterogeneous catalysts. The controversy between these two kinds of activity assessment methodologies has been comprehensively discussed in previous reviews [97,98]. To precisely evaluate the activity of nanozymes, a few alternative methodologies have been developed recently. In this section, we summarize an emerging activity assessment methodology with up-to-date advances.

Notably, the OXD-like reaction generally involves the activation of oxygen in biological processes. Another classic reaction that focuses on oxygen is the oxygen reduction reaction (ORR), which has been widely studied in the elec-

trochemical process as the rate-determining step for several decades. Inspired by their homology in activity origins, some natural oxidases have been explored as efficient oxygen reduction electrocatalysts. Correspondingly, some excellent ORR electrocatalysts are also found with enzyme-like activities. Very recently, a possible strong relationship between enzyme-like activity and ORR electrochemical activity was observed, implying the potential of using ORR as an assessment methodology to evaluate nanozyme performance.

For example, our group [99] fabricated a series of Fe–N–C nanozymes using the secondary N-containing precursor pyrolysis method (Figure 10a). The OXD-like activities assessed by TMB model chromogenic reactions revealed a volcano-like relationship with the increase of the secondary N-containing precursor amount (Figure 10b). Interestingly, by using linear voltage sweeping with a rotating disk ring electrode (RRDE) instead of using TMB as an electron donor, enhanced H_2O selectivity was observed with higher OXD-like activity (Figure 10c). This work reveals a close relationship between OXD-like activity and oxygen activation, indicating the possibility of using ORR H_2O selectivity to evaluate OXD-like activity.

In another outstanding contribution, oxidase catalysis was successfully bridged with ORR electrocatalysis. Using Cu/Fe-doped single-atom as model catalysts (Figure 10d), Shi's group [100] created CF-HNCS with outstanding OXD-like activity (Figure 10e). Notably, by using steady-state linear sweep voltammetry (LSV), the order of ORR activity shows great accordance with their OXD-like activity identified by TMB. Furthermore, the nondimensionalized velocity (v_n) and the normalized mean current density ($|j_n|$) were used to describe the OXD-like and ORR activities, respectively, demonstrating a strong linear relationship between them (Figure 10f). This work proves that the conventional ORR method is applicable to access oxidase mimics in certain circumstances.

Despite the clear relevance between ORR and OXD-like activity found in the aforementioned reports, it should be carefully employed in consideration of the nature of catalysts. For example, our group [31] synthesized Fe–N–C nanozymes with distinct graphitic structures using a pyrolysis strategy, which showed mismatched activities in driving ORR reactions and OXD-like reactions. From a kinetic point of view, ORR electrocatalysts usually need high electrical conductivity, *e.g.*, graphitic structures in doped carbon electrocatalysts to facilitate the electron transfer from the electrode to the catalyst surface and pass to oxygen (Figure 10g). However, for nanozymatic reactions, the electron exchange between oxygen and the substrate molecules confined at the catalyst surface is sufficient (Figure 10h). It indicated different principles in developing ORR electrocatalysts and nanozymes: the graphitic framework of Fe–N–C in nanozymes may not be obligatory as that for ORR.

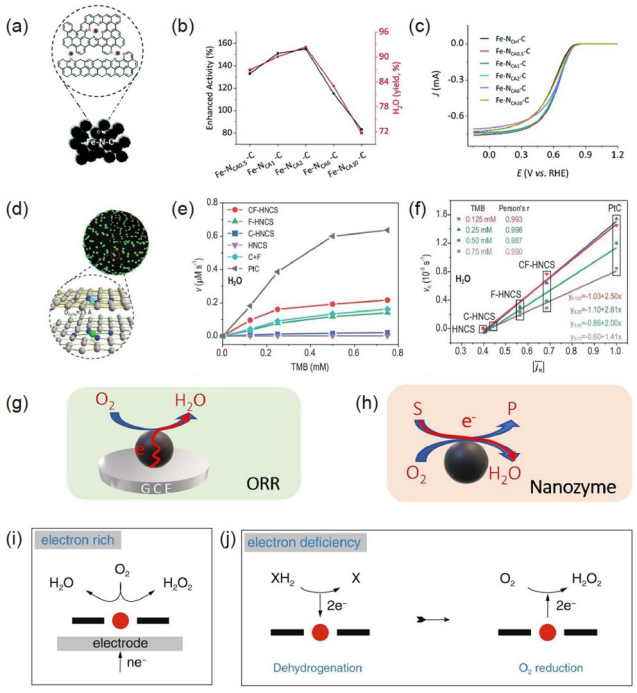

Figure 10 Emerging activity assessment methodologies bridging the OXD-like and ORR catalytic activities of nanozymes. (a) Model diagram of Fe–N–C nanozymes. (b) Enhanced OXD-like activity and H_2O selectivity at half-wave potential of a series of Fe–N–C nanozymes. (c) Linear sweep voltammograms of the Fe–N–C nanozymes. (d) Model diagram of CF-HNCS nanozymes. (e) The OXD-like activity of various nanozymes at different TMB concentrations in H_2O. (f) The linear fitting of OXD-like activity and ORR activity of nanozymes in H_2O, denoted as the non-dimensionalized velocity (v_n) and the normalized mean current density ($|j_n|$) respectively. Schematic illustration of the electron transfer and catalytic processes of nanozyme in (g) electrocatalytic ORR reaction and (h) OXD-like reaction. (i) Schematic illustration of the electron supply in electrocatalytic ORR reaction. (j) Schematic illustration of the electron supply in the enzymatic reaction is restricted by the dehydrogenation of the substrate. (a–c) reprinted with permission from ref. [99]. Copyright 2021 Royal Society of Chemistry. (d–f) reprinted with permission from ref. [100]. Copyright 2022 Oxford University Press. (g, h) reprinted with permission from ref. [31]. Copyright 2020 John Wiley and Sons. (i, j) adapted with permission from ref. [101]. Copyright 2022 Nature Publishing Group (color online).

In addition, integrating the different kinetics of ORR and OXD-like catalysis bring the improvement in selectivity. Very recently, a single-atom rhodium catalyst (Rh_1/NC) was developed to dehydrogenate various substrates and catalyzes the $2e^-$ reduction of oxygen to hydrogen peroxide with nearly 100% selectivity [101]. By re-visiting the kinetics of the electrocatalytic oxygen reduction and the enzyme-like oxygen reduction, it was found that in ORR electrocatalysis, electrons are continuously transferred from the working electrode, and thus the H_2O_2 selectivity was caused by the intrinsic properties of catalysts (Figure 10i). In enzyme-like catalysis, the supply of electrons is restricted by substrate molecule dehydrogenation. A single catalytic site on the catalyst can remove only two electrons from each substrate molecule. Consequently, O_2 can acquire only two electrons

to form H_2O_2 *via* a two-electron reduction pathway (Figure 10j).

5 Summary and outlook

Nanozymes with preeminent enzyme-like activities have become powerful candidates for natural enzyme alternatives, owing to their stability toward harsh conditions, low cost, mass-production ability, and easy purification. However, there is still challenge in activity and selectivity compared with enzymes. To close these gaps, rational structural engineering at the molecular level of nanozymes has been proven to be effective. Recently, respectable nanozymes have been synthesized with reference to natural enzyme characteristics and action patterns. Especially by mimicking the metal active sites, substrate-binding pockets, scaffolds, and allosteric regulation of natural enzymes, the catalytic performance of nanozymes has been improved by rational synthesis. Furthermore, an insightful understanding of the catalytic mechanism at the molecular level will facilitate the rational synthesis of nanozymes. In this review, we introduce the state-of-art synthesis strategy by learning from the natural enzyme counterparts and summarize the nanozyme mechanism with a particular emphasis on the adsorbed intermediates and descriptors that predict nanozyme activity. The emerging activity assessment methodology that illustrates the relationship between electrochemical oxygen reduction and enzymatic oxygen reduction is discussed with up-to-date advances.

It should be pointed out that although tremendous advances including biomimetic nanozymes have been developed to significantly improve their performance, nanozymes still face long-standing challenges of improving the activity and selectivity in a biological context as competitive alternatives to natural enzymes. In order to bridge the gap, we discuss the following challenges based on our knowledge.

(1) The activity regulation of nanozymes in a biological environment. Except for a few nanozymes that could remain highly active under physiological conditions, the activities of most nanozymes are heavily shielded in a biological environment. Currently, the activity regulation of nanozymes in a biological environment could be achieved by intrinsic structural engineering and external triggers. For the first strategy, recent advances have confirmed the efficacy of hybrid and defect structural engineering. For example, hybrid nanozymes that consist of bimetallic or metal-carbon nanomaterials show good activity under pH 7 compared with their individual component [35]. The defect structural engineering such as doping heteroatoms also renders nanozymes with enhanced activity under physiological conditions [102]. These intrinsic structural engineering strategies could channel the rapid electron transfer, and are frequently studied with enormous attention. Another strategy is to add external triggers, such as light [103–106], temperature, ultrasound, and small molecules such as metal ions, nucleoside triphosphates, and vitamins [47]. This external stimulus strategy provides feasible solutions to the real-time, responsive activity regulation of nanozymes, which is relatively less explored but has aroused increasing interest in recent years.

(2) The precise *de novo* regulation of nanozymes. (i) Designing active sites. It seems that the exposure degree and density of active sites are closely related to specific properties of nanozymes. To obtain precise atomic design of nanozymes, single-atom nanozymes have been developed with enhanced catalytic performances and controllable atomically distributed metal active sites. However, the loading efficiency and maximum atomic utilization efficiency of single atoms remain urgent. (ii) Fabricating the microenvironment of nanozymes. Enzymology has proven that the specific local physical and chemical environments of natural enzymes contribute to turnover rates, stability, and substrate selectivity. Thus, the microenvironment of nanozymes is expected to be in close proximity to that of natural enzymes. Few research involving DNA, peptides, MOFs, and carbon nanotubes have been conducted to modify the local electrostatic field and boost substrate binding. More types of nanozymes with the tailored microenvironment are in great need. In addition, the improvement of chemo-, enantio-, and site-selectivity of nanozymes are barely studied and worth noting [107]. (iii) Simulating the unique regulatory mechanism. Feedback regulation including positive/negative feedback guarantees the proper level of activity from an enzyme. The physiological significance of natural enzymes' regulatory mechanism in metabolism and homeostasis motivates the exploration of nanozymes with regulable enzyme-like activity. However, up to now, there is only little ingenious research covering allosteric regulation, making the biological content of feedback regulation under-utilized [108]. In addition, attention should be paid to the regulatory mechanism in metabolism: the regulatory mechanism must not only take into account the metabolic efficiency of each metabolic unit, but also the proper balance between each metabolic unit to guarantee the metabolic efficiency of the whole system. Thus, the nanozyme-regulatory system waits to be accomplished in the future presumably through introducing a metabolite interconversion system and compensatory control.

(3) *Operando* mechanism. The local structure of nanozymes plays a vital role in catalytic performance. Unfortunately, the real structural information is quite hard to be obtained from experiments. Moreover, the critical intermediate during the reaction process is also difficult to be identified. Recent decades have witnessed the quick development in combining experimental evidence, spectroscopy simulations, and theoretical calculations, contributing to the

disclosure of the local structure and mechanism of nanozymes. However, the complex nature of the biochemical reactions and complicated nanozyme structure call for further characterization methods. The promotion of X-ray light sources, such as synchrotron and free electron laser (FEL) may provide possibilities for making photos and movies of the nanozyme reaction process.

(4) A fundamental question to design catalysts is to figure out which property at the atomic scale determines the macroscopic kinetic. The extraordinary progress in computer-based catalyst design has unveiled the mechanism of nanozyme enzymatic activity, which mainly consists of *ab initio* and density functional theory (DFT) calculations based on first principles. However, the traditional trial-and-error method hinders the development of nanozyme design because of its laboriousness. To address these "black box"-like tentative exploration, high-throughput computational screening has been successfully applied to discover nanozymes with superoxide-dismutase [109] and hydrolases activity [110]. Very recently, promising methodologies based on machine-learning algorithms have been established to predict efficient nanozymes with high consistency [111,112]. However, there are still challenges with a large amount of all-sided experimental data and standards for nanozyme assessment techniques. Thus, establishing standardized nanozyme toolboxes is highly envisioned.

(5) The selectivity of nanozymes is still a critical issue. In addition to the intrinsic engineering strategy mentioned above, the selectivity of nanozymes can also be achieved by borrowing the working principles of the living system. For example, cascade reactions that are vital for highly efficient interconversion of diverse forms of energy in living systems to guarantee the selectivity has been successfully applied to nanozyme-only system [113].

Lastly, but not less important, beyond merely copying biologically available enzymes, for nanozymes, learning principles from biology and transferring them to industrial reactions that were not previously accessible to biology with more intriguing performance would also be fascinating [84]. Nonetheless, there still remains plenty of room to be explored and we hope this review could be desserts before dinner and attract more researchers from different backgrounds to the flourishing field of nanozymes.

Acknowledgements This work was supported by the National Natural Science Foundation of China (22174014 and 22074015) and Natural Science Foundation of Jiangsu Province (BK20220802).

Conflict of interest The authors declare no conflict of interest.

1 Gao L, Zhuang J, Nie L, Zhang J, Zhang Y, Gu N, Wang T, Feng J, Yang D, Perrett S, Yan X. *Nat Nanotech*, 2007, 2: 577–583
2 Chen J, Ma Q, Li M, Chao D, Huang L, Wu W, Fang Y, Dong S. *Nat Commun*, 2021, 12: 3375
3 Bhattacharyya S, Ali SR, Venkateswarulu M, Howlader P, Zangrando E, De M, Mukherjee PS. *J Am Chem Soc*, 2020, 142: 18981–18989
4 Dong H, Du W, Dong J, Che R, Kong F, Cheng W, Ma M, Gu N, Zhang Y. *Nat Commun*, 2022, 13: 5365
5 Singh N, NaveenKumar SK, Geethika M, Mugesh G. *Angew Chem Int Ed*, 2021, 60: 3121–3130
6 Weng Q, Sun H, Fang C, Xia F, Liao H, Lee J, Wang J, Xie A, Ren J, Guo X, Li F, Yang B, Ling D. *Nat Commun*, 2021, 12: 1436
7 Tang G, He J, Liu J, Yan X, Fan K. *Exploration*, 2021, 1: 75–89
8 Sun H, Zhao A, Gao N, Li K, Ren J, Qu X. *Angew Chem Int Ed*, 2015, 54: 7176–7180
9 Chen Y, Tian Q, Wang H, Ma R, Han R, Wang Y, Ge H, Ren Y, Yang R, Yang H, Chen Y, Duan X, Zhang L, Gao J, Gao L, Yan X, Qin Y. *Adv Mater*, 2022, 34: 2206421
10 Wei H, Gao L, Fan K, Liu J, He J, Qu X, Dong S, Wang E, Yan X. *Nano Today*, 2021, 40: 101269
11 Li S, Zhang Y, Wang Q, Lin A, Wei H. *Anal Chem*, 2022, 94: 312–323
12 Gao F, Shao T, Yu Y, Xiong Y, Yang L. *Nat Commun*, 2021, 12: 745
13 Zhang L, Zhang L, Deng H, Li H, Tang W, Guan L, Qiu Y, Donovan MJ, Chen Z, Tan W. *Nat Commun*, 2021, 12: 2002
14 Zhen W, Liu Y, Wang W, Zhang M, Hu W, Jia X, Wang C, Jiang X. *Angew Chem Int Ed*, 2020, 59: 9491–9497
15 Fan K, Xi J, Fan L, Wang P, Zhu C, Tang Y, Xu X, Liang M, Jiang B, Yan X, Gao L. *Nat Commun*, 2018, 9: 1440
16 Wang D, Zhang B, Ding H, Liu D, Xiang J, Gao XJ, Chen X, Li Z, Yang L, Duan H, Zheng J, Liu Z, Jiang B, Liu Y, Xie N, Zhang H, Yan X, Fan K, Nie G. *Nano Today*, 2021, 40: 101243
17 Liu T, Xiao B, Xiang F, Tan J, Chen Z, Zhang X, Wu C, Mao Z, Luo G, Chen X, Deng J. *Nat Commun*, 2020, 11: 2788
18 Zhao S, Li Y, Liu Q, Li S, Cheng Y, Cheng C, Sun Z, Du Y, Butch CJ, Wei H. *Adv Funct Mater*, 2020, 30: 2004692
19 Vernekar AA, Sinha D, Srivastava S, Paramasivam PU, D'Silva P, Mugesh G. *Nat Commun*, 2014, 5: 5301
20 Hao C, Qu A, Xu L, Sun M, Zhang H, Xu C, Kuang H. *J Am Chem Soc*, 2019, 141: 1091–1099
21 Cao S, Zhao Z, Zheng Y, Wu Z, Ma T, Zhu B, Yang C, Xiang X, Ma L, Han X, Wang Y, Guo Q, Qiu L, Cheng C. *Adv Mater*, 2022, 34: 2200255
22 Natalio F, André R, Hartog AF, Stoll B, Jochum KP, Wever R, Tremel W. *Nat Nanotech*, 2012, 7: 530–535
23 Ma X, Zhang L, Xia M, Li S, Zhang X, Zhang Y. *ACS Appl Mater Interfaces*, 2017, 9: 21089–21093
24 Bose I, Zhao Y. *ACS Catal*, 2021, 11: 3938–3942
25 Fan C, Tang Y, Wang H, Huang Y, Xu F, Yang Y, Huang Y, Rong W, Lin Y. *Nanoscale*, 2022, 14: 7985–7990
26 Tian Z, Yao T, Qu C, Zhang S, Li X, Qu Y. *Nano Lett*, 2019, 19: 8270–8277
27 Li F, Li S, Guo X, Dong Y, Yao C, Liu Y, Song Y, Tan X, Gao L, Yang D. *Angew Chem Int Ed*, 2020, 59: 11087–11092
28 Wang W, Luo Q, Li J, Li L, Li Y, Huo X, Du X, Li Z, Wang N. *Adv Funct Mater*, 2022, 32: 2205461
29 Li X, Huang X, Xi S, Miao S, Ding J, Cai W, Liu S, Yang X, Yang H, Gao J, Wang J, Huang Y, Zhang T, Liu B. *J Am Chem Soc*, 2018, 140: 12469–12475
30 Fedeli S, Im J, Gopalakrishnan S, Elia JL, Gupta A, Kim D, Rotello VM. *Chem Soc Rev*, 2021, 50: 13467–13480
31 Xu Y, Xue J, Zhou Q, Zheng Y, Chen X, Liu S, Shen Y, Zhang Y. *Angew Chem Int Ed*, 2020, 59: 14498–14503
32 Zhao L, Bai T, Wei H, Gardea-Torresdey JL, Keller A, White JC. *Nat Food*, 2022, 3: 829–836
33 He F, Mi L, Shen Y, Mori T, Liu S, Zhang Y. *ACS Appl Mater Interfaces*, 2018, 10: 35327–35333
34 Breslow R. *Acc Chem Res*, 2002, 28: 146–153
35 Li Y, Liu J. *Mater Horiz*, 2021, 8: 336–350
36 Wu Y, Xu W, Jiao L, Tang Y, Chen Y, Gu W, Zhu C. *Mater Today*,

2022, 52: 327–347
37 Wang Z, Zhang R, Yan X, Fan K. *Mater Today*, 2020, 41: 81–119
38 Wang D, Jana D, Zhao Y. *Acc Chem Res*, 2020, 53: 1389–1400
39 Pei J, Zhao R, Mu X, Wang J, Liu C, Zhang XD. *Biomater Sci*, 2020, 8: 6428–6441
40 Wu J, Wang X, Wang Q, Lou Z, Li S, Zhu Y, Qin L, Wei H. *Chem Soc Rev*, 2019, 48: 1004–1076
41 Jiang D, Ni D, Rosenkrans ZT, Huang P, Yan X, Cai W. *Chem Soc Rev*, 2019, 48: 3683–3704
42 Sun Y, Xu B, Pan X, Wang H, Wu Q, Li S, Jiang B, Liu H. *Coord Chem Rev*, 2023, 475: 214896
43 Xu D, Wu L, Yao H, Zhao L. *Small*, 2022, 18: 2203400
44 Ma Y, Tian Z, Zhai W, Qu Y. *Nano Res*, 2022, 15: 10328–10342
45 Zhao H, Zhang R, Yan X, Fan K. *J Mater Chem B*, 2021, 9: 6939–6957
46 Huang Y, Ren J, Qu X. *Chem Rev*, 2019, 119: 4357–4412
47 Zhang R, Fan K, Yan X. *Sci China Life Sci*, 2020, 63: 1183–1200
48 Kim MS, Lee J, Kim HS, Cho A, Shim KH, Le TN, An SSA, Han JW, Kim MI, Lee J. *Adv Funct Mater*, 2020, 30: 1905410
49 Xi J, Zhang R, Wang L, Xu W, Liang Q, Li J, Jiang J, Yang Y, Yan X, Fan K, Gao L. *Adv Funct Mater*, 2021, 31: 2007130
50 Zhang S, Li Y, Sun S, Liu L, Mu X, Liu S, Jiao M, Chen X, Chen K, Ma H, Li T, Liu X, Wang H, Zhang J, Yang J, Zhang XD. *Nat Commun*, 2022, 13: 4744
51 Zhang Z, Zhang X, Liu B, Liu J. *J Am Chem Soc*, 2017, 139: 5412–5419
52 Ouyang Y, Biniuri Y, Fadeev M, Zhang P, Carmieli R, Vázquez-González M, Willner I. *J Am Chem Soc*, 2021, 143: 11510–11519
53 Han J, Liu K, Chang R, Zhao L, Yan X. *Angew Chem Int Ed*, 2019, 58: 2000–2004
54 Wang F, Zhang Y, Du Z, Ren J, Qu X. *Nat Commun*, 2018, 9: 1209
55 Ji S, Jiang B, Hao H, Chen Y, Dong J, Mao Y, Zhang Z, Gao R, Chen W, Zhang R, Liang Q, Li H, Liu S, Wang Y, Zhang Q, Gu L, Duan D, Liang M, Wang D, Yan X, Li Y. *Nat Catal*, 2021, 4: 407–417
56 Huang L, Chen J, Gan L, Wang J, Dong S. *Sci Adv*, 2019, 5: eaav5490
57 Zhang H, Huang L, Chen J, Liu L, Zhu X, Wu W, Dong S. *Nano Energy*, 2021, 83: 105798
58 Wright AM, Wu Z, Zhang G, Mancuso JL, Comito RJ, Day RW, Hendon CH, Miller JT, Dincă M. *Chem*, 2018, 4: 2894–2901
59 Chen J, Huang L, Wang Q, Wu W, Zhang H, Fang Y, Dong S. *Nanoscale*, 2019, 11: 5960–5966
60 Liang H, Lin F, Zhang Z, Liu B, Jiang S, Yuan Q, Liu J. *ACS Appl Mater Interfaces*, 2017, 9: 1352–1360
61 Wang J, Huang R, Qi W, Su R, Binks BP, He Z. *Appl Catal B-Environ*, 2019, 254: 452–462
62 Yan X, Li H, Wang T, Li A, Zhu C, Lu G. *Chem Eng J*, 2022, 446: 136930
63 Klabunde T, Eicken C, Sacchettini JC, Krebs B. *Nat Struct Mol Biol*, 1998, 5: 1084–1090
64 Zou W, Liu Y, Li R, Guo R. *ACS Sustain Chem Eng*, 2022, 10: 10057–10067
65 Li M, Chen J, Wu W, Fang Y, Dong S. *J Am Chem Soc*, 2020, 142: 15569–15574
66 Fan L, Lou D, Wu H, Zhang X, Zhu Y, Gu N, Zhang Y. *Adv Mater Interfaces*, 2018, 5: 1801070
67 Zhang W, Dynes JJ, Hu Y, Jiang P, Ma S. *Nat Commun*, 2019, 10: 1913
68 Benedetti TM, Andronescu C, Cheong S, Wilde P, Wordsworth J, Kientz M, Tilley RD, Schuhmann W, Gooding JJ. *J Am Chem Soc*, 2018, 140: 13449–13455
69 Zhang L, Liu Z, Deng Q, Sang Y, Dong K, Ren J, Qu X. *Angew Chem Int Ed*, 2021, 60: 3469–3474
70 Wang D, Wu H, Phua SZF, Yang G, Lim WQ, Gu L, Qian C, Wang H, Guo Z, Chen H, Zhao Y. *Nat Commun*, 2020, 11: 357
71 Zhang X, Lin S, Huang R, Gupta A, Fedeli S, Cao-Milán R, Luther DC, Liu Y, Jiang M, Li G, Rondon B, Wei H, Rotello VM. *J Am Chem Soc*, 2022, 144: 12893–12900
72 Chen X, Wang Y, Dai X, Ding L, Chen J, Yao G, Liu X, Luo S, Shi J, Wang L, Nechushtai R, Pikarsky E, Willner I, Fan C, Li J. *J Am Chem Soc*, 2022, 144: 6311–6320
73 Tonga GY, Jeong Y, Duncan B, Mizuhara T, Mout R, Das R, Kim ST, Yeh YC, Yan B, Hou S, Rotello VM. *Nat Chem*, 2015, 7: 597–603
74 Wang L, Zou H, Dong Z, Zhou L, Li J, Luo Q, Zhu J, Xu J, Liu J. *Langmuir*, 2014, 30: 4013–4018
75 Zhang W, Hu S, Yin JJ, He W, Lu W, Ma M, Gu N, Zhang Y. *J Am Chem Soc*, 2016, 138: 5860–5865
76 Liu Y, Qing Y, Jing L, Zou W, Guo R. *Langmuir*, 2021, 37: 7364–7372
77 Huang X, Groves JT. *Chem Rev*, 2018, 118: 2491–2553
78 Xia H, Li N, Huang W, Song Y, Jiang Y. *ACS Appl Mater Interfaces*, 2021, 13: 22240–22253
79 Zhao C, Xiong C, Liu X, Qiao M, Li Z, Yuan T, Wang J, Qu Y, Wang XQ, Zhou F, Xu Q, Wang S, Chen M, Wang W, Li Y, Yao T, Wu Y, Li Y. *Chem Commun*, 2019, 55: 2285–2288
80 Shen X, Liu W, Gao X, Lu Z, Wu X, Gao X. *J Am Chem Soc*, 2015, 137: 15882–15891
81 Huo M, Wang L, Wang Y, Chen Y, Shi J. *ACS Nano*, 2019, 13: 2643–2653
82 Xu B, Wang H, Wang W, Gao L, Li S, Pan X, Wang H, Yang H, Meng X, Wu Q, Zheng L, Chen S, Shi X, Fan K, Yan X, Liu H. *Angew Chem Int Ed*, 2019, 58: 4911–4916
83 Zhang R, Xue B, Tao Y, Zhao H, Zhang Z, Wang X, Zhou X, Jiang B, Yang Z, Yan X, Fan K. *Adv Mater*, 2022, 34: 2205324
84 Chen X, Zhao L, Wu K, Yang H, Zhou Q, Xu Y, Zheng Y, Shen Y, Liu S, Zhang Y. *Chem Sci*, 2021, 12: 8865–8871
85 Wan K, Jiang B, Tan T, Wang H, Liang M. *Small*, 2022, 18: 2204372
86 Liang X, Han L. *Adv Funct Mater*, 2020, 30: 2001933
87 Wang Y, Zhang Z, Jia G, Zheng L, Zhao J, Cui X. *Chem Commun*, 2019, 55: 5271–5274
88 Li J, Liu W, Wu X, Gao X. *Biomaterials*, 2015, 48: 37–44
89 Wang Z, Shen X, Gao X, Zhao Y. *Nanoscale*, 2019, 11: 13289–13299
90 Nørskov JK, Abild-Pedersen F, Studt F, Bligaard T. *Proc Natl Acad Sci USA*, 2011, 108: 937–943
91 Shen X, Wang Z, Gao X, Zhao Y. *ACS Catal*, 2020, 10: 12657–12665
92 Nørskov JK, Bligaard T, Rossmeisl J, Christensen CH. *Nat Chem*, 2009, 1: 37–46
93 Wang X, Gao XJ, Qin L, Wang C, Song L, Zhou YN, Zhu G, Cao W, Lin S, Zhou L, Wang K, Zhang H, Jin Z, Wang P, Gao X, Wei H. *Nat Commun*, 2019, 10: 704
94 Wang Y, Jia G, Cui X, Zhao X, Zhang Q, Gu L, Zheng L, Li LH, Wu Q, Singh DJ, Matsumura D, Tsuji T, Cui YT, Zhao J, Zheng W. *Chem*, 2021, 7: 436–449
95 Liu Y, Zhang Y, Liu Q, Wang Q, Lin A, Luo J, Du Y, Lin YW, Wei H. *Analyst*, 2021, 146: 1872–1879
96 Lin A, Liu Q, Zhang Y, Wang Q, Li S, Zhu B, Miao L, Du Y, Zhao S, Wei H. *Anal Chem*, 2022, 94: 10636–10642
97 Zandieh M, Liu J. *Langmuir*, 2022, 38: 3617–3622
98 Gao L, Chen L, Zhang R, Yan X. *Sci Sin-Chim*, 2022, 52: 1649–1663
99 Chen X, Zhu C, Xu Y, Wang K, Cao X, Shen Y, Liu S, Zhang Y. *Catal Sci Technol*, 2021, 11: 7255–7259
100 Lu X, Gao S, Lin H, Tian H, Xu D, Shi J. *Natl Sci Rev*, 2022, 9: nwac022
101 Chen J, Ma Q, Zheng X, Fang Y, Wang J, Dong S. *Nat Commun*, 2022, 13: 2808
102 Zhang R, Yan X, Fan K. *Acc Mater Res*, 2021, 2: 534–547
103 Zhang J, Liu J. *Nanoscale*, 2020, 12: 2914–2923
104 Neri S, Garcia Martin S, Pezzato C, Prins LJ. *J Am Chem Soc*, 2017, 139: 1794–1797
105 Liu Y, Wang X, Wei H. *Analyst*, 2020, 145: 4388–4397
106 Hong Q, Yang H, Li W, Zhu CX, Fang YF, Liang SC, Cao XW, Shen

YF, Liu SQ, Zhang YJ, *ChemRxiv Preprint*, 2022, DOI: 10.26434/chemrxiv-2022-vbqkb
107 Dong K, Xu C, Ren J, Qu X. *Angew Chem Int Ed*, 2022, 61: e202208757
108 Zhu C, Zhou Z, Cao X, Xu Y, Shen Y, Liu S, Zhang Y, *ChemRxiv Preprint*, 2022, DOI: 10.26434/chemrxiv-2022-7fh2v
109 Wang Z, Wu J, Zheng JJ, Shen X, Yan L, Wei H, Gao X, Zhao Y. *Nat Commun*, 2021, 12: 6866
110 Li S, Zhou Z, Tie Z, Wang B, Ye M, Du L, Cui R, Liu W, Wan C, Liu Q, Zhao S, Wang Q, Zhang Y, Zhang S, Zhang H, Du Y, Wei H. *Nat Commun*, 2022, 13: 827
111 Zhang C, Yu Y, Shi S, Liang M, Yang D, Sui N, Yu WW, Wang L, Zhu Z. *Nano Lett*, 2022, 22: 8592–8600
112 Wei Y, Wu J, Wu Y, Liu H, Meng F, Liu Q, Midgley AC, Zhang X, Qi T, Kang H, Chen R, Kong D, Zhuang J, Yan X, Huang X. *Adv Mater*, 2022, 34: 2201736
113 Zhou Q, Yang H, Chen X, Xu Y, Han D, Zhou S, Liu S, Shen Y, Zhang Y. *Angew Chem Int Ed*, 2022, 61: e202112453